

Gamma-ray line emission from OB associations and young open clusters

II. The Cygnus region

J. Knödlseeder¹, M. Cerviño², J.-M. Le Duigou¹, G. Meynet³, D. Schaerer⁴, and P. von Ballmoos¹

¹ Centre d'Etude Spatiale des Rayonnements, CNRS/UPS, B.P. 4346, 31028 Toulouse Cedex 4, France

² LAEFF (INTA) Apdo. 50727, Madrid 28080, Spain

³ Observatoire de Genève, CH-1290 Sauverny, Switzerland

⁴ Observatoire Midi-Pyrénées, 14, avenue Edouard Belin, 31400 Toulouse, France

Received / Accepted

Abstract. Gamma-ray and microwave observations of the Cygnus region reveal an intense signal of 1.809 MeV line emission, attributed to radioactive decay of ²⁶Al, that is closely correlated with 53 GHz free-free emission, originating from the ionised interstellar medium. We modelled both emissions using a multi-wavelength evolutionary synthesis code for massive star associations that we applied to the known massive star populations in Cygnus. For all OB associations and young open clusters in the field, we determined the population age, distance, and richness as well as the uncertainties in all these quantities from published photometric and spectroscopic data. We propagate the population uncertainties in model uncertainties by means of a Bayesian method. The young globular cluster Cyg OB2 turns out to be the dominant ²⁶Al nucleosynthesis and ionisation source in Cygnus. Our model reproduces the ionising luminosity of the Cygnus region very well, yet it underestimates ²⁶Al production by about a factor of 2. We attribute this underestimation to shortcomings of current nucleosynthesis models, and suggest the inclusion of stellar rotation as possible mechanism to enhance ²⁶Al production. We also modelled ⁶⁰Fe nucleosynthesis in the Cygnus region, yet the small number of recent supernova events suggests only little ⁶⁰Fe production. Consequently, a detection of the 1.137 MeV and 1.332 MeV decay lines of ⁶⁰Fe from Cygnus by the upcoming *INTEGRAL* observatory is not expected.

Key words. nucleosynthesis – OB associations – young open clusters – Cygnus – ²⁶Al – ⁶⁰Fe

1. Introduction

OB associations and young open clusters constitute the most prolific nucleosynthesis sites in our Galaxy. The combined activity of stellar winds and core-collapse supernovae ejects significant amounts of freshly synthesised nuclei into the interstellar medium. Radioactive isotopes, such as ²⁶Al or ⁶⁰Fe, that have been co-produced in such events may eventually be observed by gamma-ray instruments through their characteristic decay-line signatures. Indeed, galactic 1.809 MeV gamma-ray line emission attributed to the radioactive decay of ²⁶Al has been observed by numerous gamma-ray telescopes (see Prantzos & Diehl 1996 for a review). In particular, the COMPTEL telescope provided the first image of the Galaxy in the light of this isotope, showing an asymmetric ridge of diffuse emission along the galactic plane with a prominent localised emission enhancement in the Cygnus region (Diehl et al. 1995).

The Cygnus emission has been interpreted as the result of ²⁶Al ejection in Wolf-Rayet winds and during core collapse supernova explosions from a nearby (1-2 kpc) massive star population which probably is part of the local spiral arm structure (del Rio et al. 1996).

Gamma-ray line emission is not the only tracer of this activity. Knödlseeder et al. (1999a) demonstrated that the galactic 1.809 MeV emission is closely correlated to galactic free-free emission as observed in the microwave domain. The free-free emission mainly results from the ionisation of the interstellar medium by the UV flux of O stars, hence it traces the massive star population. The observed correlation is indeed one of the strongest arguments in favour of prolific ²⁶Al production by massive stars. In general, a wealth of distinct massive star populations of different ages, sizes, or metallicities contribute to the emission along a line of sight through the Galaxy, and the observed correlation allows only conclusions about the average properties of the contributing populations. In that way, the observations suggest that the equivalent O7V star

^{26}Al yield, defined as the average amount of ^{26}Al ejected per number of O7V star (measured by their equivalent ionising production), has a galaxywide constant value of $Y_{26}^{\text{O7V}} = (1.0 \pm 0.3) \times 10^{-4} M_{\odot}$ (Knödlseher 1999).

It is surprising, however, that the correlation between 1.809 MeV and microwave free-free emission also holds for the Cygnus region. Both gamma-ray and microwave data show a localised emission enhancement towards Cygnus, similar in size and relative intensity, resulting in an equivalent O7V star ^{26}Al yield of $(1.1 \pm 0.3) \times 10^{-4} M_{\odot}$ (see Sect. 4). Within the uncertainties this yield is identical to the galactic value. In contrast to the Galaxy, however, only few massive star associations contribute to the observed emission in Cygnus, and it is not expected that they have the same properties as the Galaxy as a whole. In particular, the galactic metallicity gradient leads to an average galactic abundance that is supersolar, and indeed only a supersolar abundance is able to reconcile theoretical ^{26}Al yields with the observed galactic ^{26}Al mass (Knödlseher 1999). In contrast, massive star populations in Cygnus show slightly subsolar abundances (e.g. Daffon et al. 2001) and since ^{26}Al yields are believed to depend on metallicity (e.g. Prantzos & Diehl 1996) the nucleosynthetic properties of the Cygnus region should deviate from those of the average Galaxy.

To understand the observations, we present in this paper a bottom-up model of the Cygnus region where we aim to explain the gamma-ray and microwave data from the underlying stellar populations. For this purpose we developed a multi-wavelength evolutionary synthesis model that we presented in paper I of this series (Cerviño et al. 2000). We put considerable effort into the characterisation of the massive star populations in Cygnus with particular emphasis on the involved uncertainties (distance and age uncertainty; coeval or continuous star formation). We incorporate these uncertainties into our model by means of a Bayesian method and determine confidence intervals for all quantities to assess the predictive power of our approach. Despite the resulting uncertainties, we will demonstrate that the gamma-ray observations provide important clues on nucleosynthesis physics in massive stars. In particular we will demonstrate the shortcomings of current theoretical nucleosynthesis models in explaining ^{26}Al production and discuss possible modifications that may improve the models.

2. Evolutionary synthesis model and analysis method

The evolutionary synthesis model we employed in this work is described in detail in the first paper of this series by Cerviño et al. (2000). In summary, the evolution of each individual star in a stellar population is followed using Geneva evolutionary tracks with enhanced mass-loss rates (Meynet et al. 1994). Stellar Lyman continuum (Lyc) luminosities are predicted using the CoStar atmosphere models of Schaerer & de Koter (1997), supplemented by the Schmutz et al. (1992) atmospheres for

the Wolf-Rayet phase. At the end of stellar evolution, stars initially more massive than $M_{\text{WR}} = 25 M_{\odot}$ are exploded as Type Ib supernovae, while stars of initial mass within $8M_{\odot}$ and M_{WR} are assumed to explode as Type II SNe. Nucleosynthesis yields have been taken from Meynet et al. (1997) for the pre-supernova evolution, from Woosley & Weaver (1995) for Type II and from Woosley et al. (1995) for Type Ib supernova explosions. Note that Type II SN yields have only been published for stars without mass loss and Type Ib yields have only been calculated for pure Helium stars. In order to obtain consistent nucleosynthesis yields for Type II supernovae we followed the suggestion of Maeder (1992) and linked the explosive nucleosynthesis models of Woosley & Weaver (1995) to the Geneva tracks via the carbon-oxygen core mass at the beginning of carbon burning. For Type Ib SN we used the helium-core mass at the beginning of helium core burning for the link.

In order to predict the present gamma-ray line emission from a massive star association we have to estimate the production of radioactive isotopes in the past. We do this by determining the actual number of stars N_* within a given initial mass interval $[M_{\text{low}}, M_{\text{up}}]$ that is not affected by incompleteness at the lower end and evolutionary effects at the upper end. We then extrapolate this population back to the past using a Salpeter initial mass function (IMF) of slope $\Gamma = -1.35$ that is normalised to the number of stars we observe today. In practice, we generate an initial stellar population by randomly sampling the IMF until the number of stars falling in the mass interval $[M_{\text{low}}, M_{\text{up}}]$ amounts to N_* . We then use the evolutionary synthesis code to follow the time evolution of the ^{26}Al and ^{60}Fe yields, the Lyc luminosity, and the distribution of spectral types within the population.

The stellar systems we study in this work only comprise a few hundred to a few thousand stars, making the high-mass end of the population generally sparsely sampled. However, massive stars provide a considerable fraction of the association nucleosynthesis and ionising power, and the early evolution of the system will depend rather sensitively on the actual choice of stellar masses. In particular, different Monte Carlo samples of the same initial stellar population may lead to quite different evolutions of the association observables, leading to considerable uncertainties in our model predictions. We decided to include these uncertainties in our analysis by means of a Bayesian method. Instead of investigating the time evolution of a quantity X for a specific population, we base our analysis on the probability density function (PDF) $p(X|t)$ which quantifies the probability for X to be equal to a value x at the time t . We approximate this function for a given association by repeating the evolutionary synthesis calculations for independently sampled stellar populations, from which we obtain the frequency of observing the value x at time t . In this way, the uncertainty arising from the extrapolation to the past, which manifests in an uncertainty about the initial massive star population, is reflected in the width of the PDF. Examples of PDFs obtained for

massive star associations in the Cygnus regions are given in Cerviño et al. (2000).

To predict the today value of the quantity X , we marginalise over the (uncertain) age t of the association using

$$p(X) = \int_0^\infty p(t)p(X|t)dt, \quad (1)$$

where the prior probability distribution $p(t)$ quantifies the age uncertainty. We tried different choices for the prior distributions, such as Gaussians or bounded uniform functions, but we found that the precise form of the prior has little impact on the result as long as it quantifies our knowledge about the age uncertainty (see Sect. 4.2.1). To estimate fluxes S_i from luminosities L_i for a given association i , we further marginalise over the distance s of the association using

$$p_i(S_i) = \int_0^\infty p(s)p(L_i|s)ds. \quad (2)$$

where the prior $p(s)$ quantifies the distance uncertainty, and $S_i \propto s^{-2}$. Integral fluxes from the Cygnus region were obtained by adding the contributions from individual OB associations and young open clusters using successive marginalisation, i.e.

$$p(S) = \int_0^\infty p_1(S_1)p_2(S - S_1)dS_1, \quad (3)$$

where p_1 and p_2 are the flux PDFs for association 1 and 2, respectively, and $S = S_1 + S_2$. Finally, we derive mean (or median) flux values and 63.8 % confidence regions from these PDFs which we then compare to observations.

3. Massive star populations in Cygnus

The starting point of our study of massive star populations in Cygnus is the WEBDA database of open clusters of Mermilliod (1998). From this database we established a list of open clusters within the limits $60^\circ < l < 110^\circ$ and $|b| < 15^\circ$, a region which largely encloses the 1.809 MeV and microwave free-free emission features. We preselected young clusters from this list by requiring either an earliest spectral type of B3V or earlier (corresponding to a star of $\sim 8 M_\odot$ initial mass), or a cluster age of less than 5×10^7 yr. Older clusters do not house any potential core collapse progenitor anymore, and their nucleosynthesis activity is therefore negligible. The lack of stars more massive than $\sim 10 M_\odot$ also reduces their ionising flux to an imperceptible level. Of course, not for all known open clusters an age estimate is available, but those clusters are then often rather distant and/or do not contain luminous members. Consequently, they do not contribute significantly to the emissions that we aim to study in this work.

For the OB associations in the Cygnus region we gathered the relevant information from the literature. Our main resources were the compilations of Humphreys (1978) and Garmany & Stencel (1992), complemented with data from the SIMBAD database and

some recent investigations (see the appendix for a detailed description of our database).

The association parameters relevant to our study are the age τ , the distance d , the richness, expressed as the number of stars N_* in a specific initial mass interval $[M_{\text{low}}, M_{\text{up}}]$, and the slope Γ of the IMF (in the following we deliberately choose the term association when we talk both about OB associations and young open clusters). Literature values for these parameters are only available for some of the associations, and have generally been derived by different methods. Also the choice of the stellar evolutionary tracks and luminosity calibrations impacts the results, and may lead to differences among the derived parameters. Additionally, the uncertainty of the association parameters has rarely been determined, and if so, also not in a consistent manner. For these reasons we decided to re-determine the relevant association parameters and their uncertainties from the basic stellar data in our database. In the following we describe our method and present the resulting parameters for all young stellar associations in Cygnus. The results of the analysis are summarised in Tables 1 and 2. Details for each association are given in the appendix.

3.1. Reddening

As a first step we determine the reddening for each association from spectroscopic and photometric information. For each star with spectral classification we used the spectral type to intrinsic colour calibration of FitzGerald (1970) complemented by information from Schmidt-Kaler (1982) for the earliest spectral types to determine their colour excess $E(B - V) = (B - V) - (B - V)_0$ and $E(U - B) = (U - B) - (U - B)_0$. From these we calculate the slope $q_r = E(U - B)/E(B - V)$ of the reddening curve for each association by averaging the slopes of all member stars with known spectral type. Outliers were iteratively removed from the average until all remaining stars lie within 2 rms of the average.

The slopes typically vary from 0.67 to 0.84 with a few exceptions with poorly defined values due to the proximity of the association (Cyg OB7, Lac OB1, Roslund 5). We find a trend towards steeper slopes (typically around $q_r = 0.80$) for the more reddened associations, in particular in the area of Cyg OB1, OB2 and OB9, i.e. the central part of the Cygnus X region. This confirms findings by other authors (e.g. Massey & Thompson 1991) of an anomalous reddening in this area. For the couple of open clusters for which no spectral data are available, the canonical value of $q_r = 0.72$ has been adopted. In view of the dispersion in the value of q_r in the Cygnus area this choice is certainly somewhat arbitrary, but the impact of the exact value on the resulting cluster parameters is rather small, leading to a negligible additional uncertainty in our study.

Table 1. Reddening and distance moduli for OB associations and young open clusters in the field $60^\circ < l < 110^\circ$, $-15^\circ < b < 15^\circ$. Columns 5 and 6 specify the selection criteria that were applied to remove field or background stars from the datasets. Column 7 indicates the possible physical relation of an open cluster to an OB association as suggested by our analysis (see details in the appendix).

Name	q_r	DM	$E(B - V)$	$E(B - V)$ range	ΔDM	Association
Cep OB1	0.75 ± 0.03	12.8 ± 0.4	0.60 ± 0.16	-	-	
Cep OB2	0.79 ± 0.13	9.1 ± 0.3	0.49 ± 0.14	-	-	
Cyg OB1	0.80 ± 0.04	11.4 ± 0.4	0.74 ± 0.15	-	0.8	
Cyg OB2	0.79 ± 0.02	11.0 ± 0.5	1.84 ± 0.29	1.2 – 5.0	0.8	
Cyg OB3	0.73 ± 0.04	11.7 ± 0.7	0.49 ± 0.12	-	-	
Cyg OB7	0.66 ± 0.20	9.6 ± 0.2	0.36 ± 0.23	-	-	
Cyg OB8	0.77 ± 0.04	11.9 ± 0.5	0.97 ± 0.33	-	-	
Cyg OB9	0.81 ± 0.06	10.5 ± 0.4	1.12 ± 0.26	-	-	
Lac OB1	0.58 ± 0.31	9.0 ± 0.5	0.12 ± 0.03	-	-	
Vul OB1	0.69 ± 0.06	11.9 ± 0.2	0.92 ± 0.07	0.8 – 1.1	0.8	
Berkeley 86	0.79 ± 0.05	11.1 ± 0.3	0.96 ± 0.12	-	0.6	Cyg OB1
Berkeley 87	0.84 ± 0.03	11.4 ± 1.0	1.63 ± 0.13	-	-	Cyg OB1
Berkeley 94	0.72	13.6 ± 0.1	0.68 ± 0.06	-	-	
Berkeley 96	0.72	13.6 ± 0.1	0.65 ± 0.04	-	-	
Biurakan 2	0.72	11.8 ± 0.4	0.47 ± 0.08	0.2 – 0.7	0.8	Cyg OB3 (?)
IC 4996	0.78 ± 0.12	11.1 ± 0.3	0.68 ± 0.06	0.5 – 0.8	1.0	Cyg OB1
IC 5146	0.72 ± 0.18	10.3 ± 1.0	0.64 ± 0.34	0.3 – 1.2	1.2	
NGC 6823	0.70 ± 0.08	12.1 ± 0.4	0.86 ± 0.14	0.5 – 1.2	0.8	Vul OB1
NGC 6871	0.81 ± 0.09	11.9 ± 0.4	0.45 ± 0.02	0.4 – 0.6	0.6	Cyg OB3
NGC 6883	0.72	11.3 ± 0.7	0.39 ± 0.04	-	-	Cyg OB3 (?)
NGC 6910	0.80 ± 0.06	11.3 ± 0.5	1.12 ± 0.09	0.9 – 1.25	0.8	
NGC 6913	0.80 ± 0.15	11.3 ± 1.0	0.91 ± 0.14	0.6 – 1.5	-	Cyg OB1
NGC 7067	0.72	14.2 ± 0.1	0.90 ± 0.10	-	-	
NGC 7128	0.72	13.2 ± 0.4	1.05 ± 0.06	0.7 – 1.3	0.8	
NGC 7160	0.73 ± 0.16	10.0 ± 0.4	0.35 ± 0.04	0.2 – 0.8	0.6	
NGC 7235	0.67 ± 0.06	12.8 ± 0.4	0.92 ± 0.04	0.7 – 1.1	0.8	Cep OB1
NGC 7261	0.72	12.8 ± 0.4	1.04 ± 0.10	0.8 – 1.4	0.8	Cep OB1
NGC 7380	0.78 ± 0.06	12.8 ± 0.2	0.60 ± 0.04	0.5 – 0.9	0.8	Cep OB1
Roslund 4	0.72	12.3 ± 0.6	1.05 ± 0.15	-	-	
Roslund 5	1.15 ± 0.16	8.6 ± 0.3	0.10 ± 0.04	-	-	
Ruprecht 175	0.63 ± 0.18	11.3 ± 0.1	0.26 ± 0.03	-	-	
Trumpler 37	0.71 ± 0.07	10.2 ± 0.4	0.54 ± 0.08	0.2 – 1.0	0.8	

3.2. Distance

As a second step the distance of each association is estimated. For associations with spectroscopic information we employed the method of spectroscopic parallax. For each MK classified star we compute $DM = V - A_V - M_V$, where $A_V = R_V \times E(B - V)$ is the visible extinction. The association distance is then calculated by averaging DM where again 2 rms outliers were removed iteratively. The absolute visual magnitudes M_V have been extracted from calibrations of Vacca et al. (1996) for stars earlier than B1, complemented by data from Humphreys & McElroy (1984) and Schmidt-Kaler (1982) for later spectral types. For the ratio R_V of absolute-to-selective absorption we apply the canonical value of 3.1, although we recognise that deviations from this value are eventually observed in star forming regions (Mathis 1990). For Cyg OB2, for example, Massey & Thompson (1991) found $R_V = 3.0$, and indeed a variable extinction analysis of our data suggests a similar

value. This deviation results in a distance modulus error of 0.2 mag for this association, inferior to the statistical and systematical uncertainty of 0.5 mag. Cyg OB2 is certainly an extreme case due to the large reddening of the association, and we believe that variations in R_V should not dramatically alter our results. Anyways, we have little choice since generally the available data do not allow to perform a reliable variable extinction analysis for the associations, and we fear that a poorly determined value of R_V introduces a larger error than a rather solid mean value of 3.1 that may not precisely apply to all cases.

For some of the open clusters for which not enough spectral type information was available, we estimated the distance from the hot cluster stars using the reddening-free parameter $Q = (U - B) - q_r \times (B - V)$, where q_r is the mean cluster reddening slope as given in Table 1. For $Q < -0.4$, corresponding to spectral types earlier than B5 or so, there exist unique relations between intrinsic

colour $(B - V)_0$, absolute visual magnitude M_V , and Q for each luminosity class. We determined these relations by fitting polynomial functions to calibration tables that we compiled from FitzGerald (1970), Schmidt-Kaler (1982), Humphreys & McElroy (1984), and Vacca et al. (1996). To estimate the luminosity class we apply an iterative approach. For each star with $Q < -0.4$ we assume as initial estimate a luminosity class of V (this is certainly a reasonable assumption for young unevolved clusters). Based on this estimate we use the calibration relations to determine $(B - V)_0$ and M_V from Q . From these quantities we derive $E(B - V)$, A_V , and DM , leading to a first cluster distance estimate by averaging over DM . Cluster stars which we misclassified in luminosity class will clearly show up as outliers in DM with respect to the average. Hence, for stars with DM more than 1 rms above the average we reduce the luminosity class (in the sense $V \rightarrow I$) while for stars with DM more than 1 rms below the average we increase the luminosity class (in the sense $I \rightarrow V$) for the next iteration. We then repeat the entire procedure for the updated luminosity classes. For all clusters in our sample, this scheme led to convergence in DM after 2 – 3 iterations. We tested the validity of our procedure by applying the method to clusters for which DM is known from spectroscopic parallaxes and found satisfactory agreement with the photometric results.

3.3. Field star separation

For Cyg OB2 and many of the clusters, field star contamination is a serious problem in our database. Field stars may be recognised by particularly low or high $E(B - V)$ values with respect to bona fide association members (e.g. Massey et al. 1995). For contaminated associations, we therefore excluded those stars whose inferred colour excess is outside the range spanned by member stars with MK classification. Most clusters show a clear upper main sequence which allows for an unambiguous definition of stellar reddenings of cluster members. For the cases where we applied such a selection, the $E(B - V)$ range of cluster members is specified in column 5 of Table 1.

To perform such a selection, $E(B - V)$ has been determined for each star from either spectroscopic or photometric data. In the latter case, the iterative procedure described above has been used for hot stars with $Q < -0.4$. For $Q \geq -0.4$, the relation between $(B - V)_0$ and Q becomes ambiguous, corresponding to the well known ‘knee’ in the colour-colour diagram. Nevertheless, from the intersection of the reddening lines with the intrinsic colour-colour tracks we can determine all possible $E(B - V)$ values (3 at maximum) that are consistent with the observed colours, and we exclude all stars that have no solution that is compatible with the specified colour excess interval.

To remove remaining field or background stars we employed for most clusters another selection criterion based on the distance moduli of the stars. From bona fide members with MK classification we define a distance

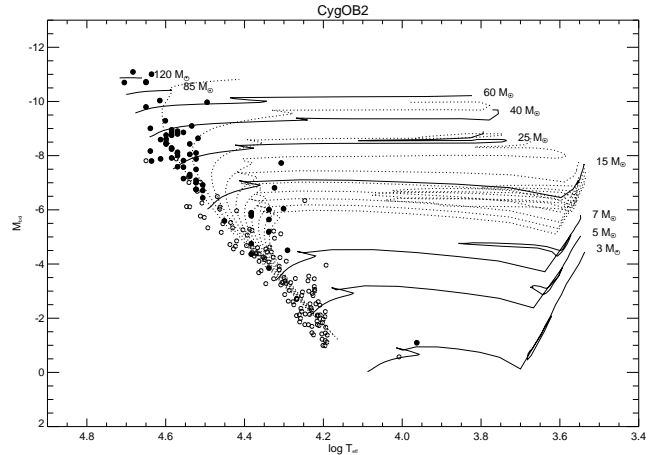


Fig. 1. H-R diagram of Cyg OB2. The filled circles are stars for which spectral classification is available, the open circles are stars for which we have only photometry. Solid lines are the stellar tracks of Meynet et al. (1994), dotted lines are the corresponding isochrones for intervals of 2 Myr, starting from $\tau = 2$ Myr.

moduli interval ΔDM and exclude all stars for which $|DM - \langle DM \rangle| > \Delta DM$, where $\langle DM \rangle$ is the distance modulus of the association. Distance moduli for stars with MK classification or hot ($Q < -0.4$) stars were determined from spectroscopic and photometric parallaxes, respectively. For the remaining stars, distance moduli were again estimated from the intersection of the reddening lines with the intrinsic colour-colour tracks.

3.4. Transformation to $\log T_{\text{eff}}$ and M_{bol}

Our next step consists of constructing H-R diagrams (HRDs) for all associations. For this purpose we transform the spectroscopic and photometric information for all member stars to $\log T_{\text{eff}}$ and M_{bol} . If a star has a MK classification, we used the spectral type to determine both the effective temperature and bolometric correction $B.C.$ using the calibration of Vacca et al. (1996), complemented by data from Humphreys & McElroy (1984) and Schmidt-Kaler (1982). From the absolute visual magnitude and the bolometric correction, the bolometric luminosity is then derived using $M_{\text{bol}} = M_V + B.C.$

For stars without MK classification, we again distinguish between hot ($Q < -0.4$) and cold ($Q \geq -0.4$) stars. For hot stars we determined $\log T_{\text{eff}}$ and $B.C.$ from Q , while for cold stars we derived both parameters from the intrinsic colour $(B - V)_0$. Using the mean association distance DM and extinction A_V we assign a bolometric luminosity to each star using $M_{\text{bol}} = V - A_V - DM + B.C.$ We estimate the intrinsic colour $(B - V)_0 = (B - V) - E(B - V)$ for each star by assuming a reddening identical to the mean reddening of the association. Our analysis is based on polynomial functions that we fitted to the calibration tables of intrinsic stellar parameters. In general, the relations depend of the luminosity class which we esti-

Table 2. Population parameters for the associations of Table 1 (IC 5146 which is older than 50 Myr has been excluded). Columns 3 and 4 list the number of O and WR stars within the association, columns 5-7 give the WR subtype distribution. The 120 O stars quoted for Cyg OB2 are probably an upper limit (see text) while the belonging of the O star 10 Lac to Lac OB1 is questionable (see appendix). The WR identifications are given in the last column. The physical reality of the associations marked by * is extremely doubtful. The last row summarises the stellar statistics for the entire region.

Name	age (Myr)	N_O	N_{WR}	N_{WN}	N_{WC}	N_{WO}	N_*	$[M_{low}, M_{up}]$	WR
Cep OB1a	2 – 5	18	4	3	1	-	16	[20, 40]	152,153,154,155
Cep OB1b	9 – 18	-	-	-	-	-	19	[9, 15]	
Cep OB2	10 – 16	-	-	-	-	-	9	[7, 12]	
Cyg OB1	2 – 6	11	4	3	1	-	23	[15, 40]	136,137,138,141
Cyg OB2	1 – 4	(120)	3	1	2	-	120	[20, 120]	144,145,146
Cyg OB3	2 – 5	12	2	1	1	-	14	[25, 60]	134,135
Cyg OB7	2 – 5	2	-	-	-	-	10	[7, 25]	
Cyg OB8*	1 – 14	6	-	-	-	-	8	[20, 40]	
Cyg OB9	2 – 5	8	-	-	-	-	6	[20, 40]	
Lac OB1	12 – 15	(1)	-	-	-	-	14	[7, 12]	
Vul OB1*	2 – 6	3	-	-	-	-	5	[15, 40]	
Berkeley 86	3 – 5	2	1	1	-	-	11	[7, 25]	139
Berkeley 87	3 – 6	2	1	-	-	1	24	[7, 25]	142
Berkeley 94	3 – 5	1	-	-	-	-	4	[7, 15]	
Berkeley 96	4 – 7	1	-	-	-	-	3	[7, 15]	
Biurakan 2	24 – 30	-	-	-	-	-	12	[4, 9]	
IC 4996	4 – 7	2	-	-	-	-	6	[7, 25]	
NGC 6823	1 – 5	4	-	-	-	-	21	[7, 20]	
NGC 6871	5 – 6	-	1	1	-	-	13	[7, 25]	133
NGC 6883	14 – 16	-	-	-	-	-	2	[12, 15]	
NGC 6910	4 – 5	2	-	-	-	-	7	[7, 25]	
NGC 6913	2 – 5	3	-	-	-	-	13	[7, 40]	
NGC 7067	14 – 18	-	-	-	-	-	27	[5, 9]	
NGC 7128	26 – 30	-	-	-	-	-	27	[4, 7]	
NGC 7160	8 – 14	-	-	-	-	-	4	[5, 7]	
NGC 7235	4 – 5	-	-	-	-	-	18	[7, 15]	
NGC 7261	12 – 20	-	-	-	-	-	17	[5, 12]	
NGC 7380	4 – 5	1	-	-	-	-	8	[7, 20]	
Roslund 4	5 – 15	-	-	-	-	-	6	[7, 12]	
Roslund 5	20 – 30	-	-	-	-	-	6	[3, 5]	
Ruprecht 175	20 – 30	-	-	-	-	-	3	[3, 5]	
Trumpler 37	3 – 6	5	-	-	-	-	25	[7, 25]	
total		204	16	10	5	1			

mate for each star from the absolute visual magnitude $M_V = V - A_V - DM$ (unless it has already been estimated by the iterative procedure described in §3.2). Here we make use of the rapid variation of M_V with luminosity class, and we search the calibration tables for the luminosity class that comes closest to the pair M_V and $(B - V)_0$ of stellar parameters. Although this method is certainly not very accurate, the impact of a misclassification in luminosity class is only moderate. Typically, $\log T_{\text{eff}}$ varies about 0.02–0.1 dex and $B.C.$ about 0.3–0.7 mag between subsequent luminosity classes.

3.5. Age determination

From the H-R diagrams we estimated the age of the associations. For this purpose we compared the location of the association stars in the HRDs to the theoretical evolutionary tracks of Meynet et al. (1994) for solar metallicity ($Z = 0.02$). The same tracks are used for the evolutionary synthesis calculations, hence in this respect our models are consistent with the population input data. As an example we show the HRD for Cyg OB2 in Fig. 1 which may be compared to Fig. 16 of Massey & Thompson (1991) who made a similar analysis. From the upper part of the HRD (masses $\gtrsim 20 M_\odot$) we infer the ages of the massive stars from the Meynet et al. (1994) isochrones that we superimposed on the diagrams. For Cyg OB2, for example, this

Table 3. IMF slopes Γ for two OB associations and some open clusters. The third column indicates the mass range over which the slope has been determined.

Name	Γ	mass range (M_{\odot})
Cyg OB1	-1.0 ± 0.4	15 – 85
Cyg OB2	-1.1 ± 0.3	15 – 120
Berkeley 86	-1.2 ± 0.5	7 – 40
Berkeley 87	-1.2 ± 0.4	7 – 60
IC 4996	-1.6 ± 0.5	5 – 40
NGC 6823	-1.3 ± 0.4	7 – 60
NGC 6871	-1.0 ± 0.5	7 – 40
NGC 6910	-0.9 ± 0.4	5 – 40
NGC 6913	-0.6 ± 0.5	7 – 60
NGC 7235	-2.6 ± 0.6	7 – 40
NGC 7380	-0.9 ± 0.5	7 – 40
Trumpler 37	-1.1 ± 0.4	7 – 60

method leads us to an age estimate of 1 – 4 Myr, comparable to the finding of Herrero et al. (1999).

The results for all associations are summarised in Table 2. Instead of determining a best fitting age, we always tried to specify an age range that reflects the dispersion of the upper main sequence. The dispersion comes partly from the systematic limitation of our method (knowledge of stellar calibrations, neglect of stellar rotation and binarity, measurement or classification errors), but could also reflect a period of continuous star formation. In particular, some associations like Cep OB1, Cyg OB8 or Roslund 4 show a considerable scatter in the upper HRD which could even reflect several epochs of massive star formation. For Cep OB1 we decided to split the population into two subgroups of different age since the data are difficult to reconcile with a single star formation event. Yet, a large apparent age spread could also signal that the association presents not a physically associated group but rather a chance projection of massive stars in the sky. For this reason we excluded Cyg OB4 from our study since *Hipparcos* data did not confirm the reality of this stellar group (de Zeeuw et al. 1999). Other associations such as Cyg OB8 or Vul OB1 are also highly doubtful, yet it will turn out that they provide only a negligible contribution to the overall luminosities in the Cygnus region, hence we do not introduce an important uncertainty by including them into our study.

3.6. Association richness and IMF

The comparison of the H-R diagram with the evolutionary tracks allows an estimation of the initial richness of the association. We determined the richness by counting the number of stars N_* over a sufficiently large initial mass interval $[M_{\text{low}}, M_{\text{up}}]$. We tried to choose the lower mass limit M_{low} sufficiently high to avoid any bias from population incompleteness due to the limiting magnitudes of the association surveys. Conversely, the upper mass limits

M_{up} were chosen sufficiently low so that the evolutionary turn-off has no impact on the richness determination. The results are summarised in columns 8 and 9 of Table 2.

The only exception to this procedure is Cyg OB2 for which we rely on the recent mass determination of Knödlseeder (2000), based on an analysis of *2MASS* near infrared data. In fact, the data that are available in the visible waveband for Cyg OB2 are heavily affected by interstellar absorption, and their use would considerably underestimate the total mass of this association. In contrast, the *2MASS* data do not allow a precise spectral type determination and the quoted number of 120 O stars rather reflects the fact that there were initially 120 stars more massive than $\sim 20M_{\odot}$ in Cyg OB2, although some may already have evolved, having either turned in early B-type or even Wolf-Rayet stars. The quoted number of 120 O stars should therefore present an upper limit.

For some associations our stellar database contains enough objects to allow an estimation of the initial mass spectrum. We fitted these spectra by power-law initial mass functions and summarise their slopes Γ in Table 3. We also quote the mass intervals that have been used for the fitting which again were chosen to minimise any bias due to evolved stars, population incompleteness, and field star contamination. Yet we recognise that the results are still affected by systematic uncertainties, as demonstrated by the steep slope of $\Gamma = -2.6 \pm 0.6$ for NGC 7235 which shows a heavy field star contamination (Massey et al. 1995). Formally, we derive a weighted mean IMF slope of $\Gamma = -1.2 \pm 0.1$ which is close to the canonical Salpeter value of -1.35 and compatible with the value of $\Gamma = -1.12 \pm 0.08$ that has been determined by Massey et al. (1995) for 12 galactic OB associations and open clusters. To illustrate the systematic uncertainties in IMF slope determinations, we compare our result for Cyg OB2 (-1.1 ± 0.3) to the value of -1.0 ± 0.1 determined by Massey & Thompson (1991) from the same stellar data, and the recent analysis of Knödlseeder (2000) of *2MASS* near infrared data that suggests $\Gamma = -1.6 \pm 0.1$. In view of these uncertainties, we believe that the assumption of a uniform canonical Salpeter law for our evolutionary synthesis modelling of all associations is a reasonable approximation that is compatible with the observational data.

3.7. The Cygnus superbubble

The discovery of an extended X-ray ring-like source surrounding the Cygnus X region by Cash et al. (1980) has been interpreted as a superbubble blown by the massive star winds and supernova explosions in the Cyg OB2 association. Anomalous stellar proper motions have been reported for stars in associations located near the edge of the bubble (Comerón et al. 1993), and have been interpreted as the sign for triggered star formation following gravitational instability of the expanding shell (Comerón & Torra 1994). However, the energetic requirements needed to explain the expansion motion are difficult to reconcile with

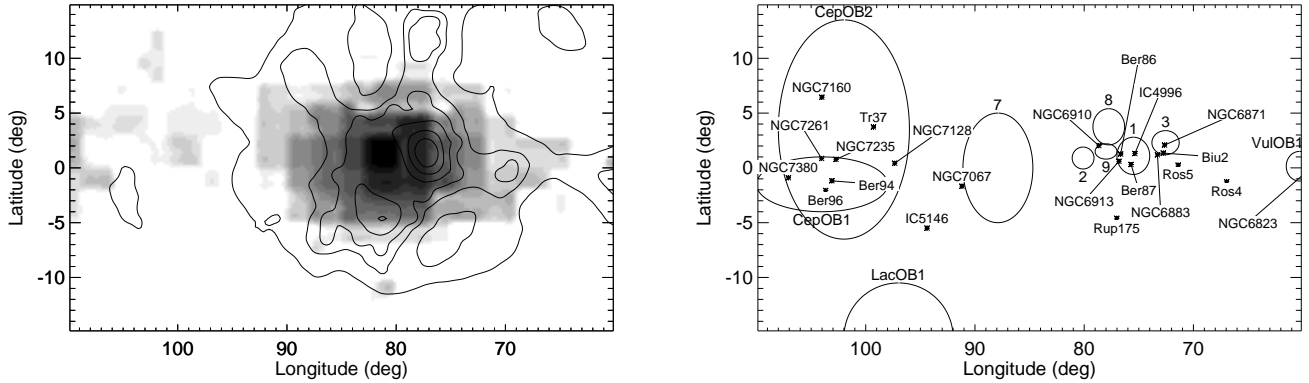


Fig. 2. *Left:* Contour map of 1.809 MeV gamma-ray line emission in the Cygnus region (Plüschke 2001) superimposed onto a greyscale image of microwave 53 GHz free-free emission (Bennett et al. 1992). The prominent emission feature extending from $l \sim 70^\circ$ to 90° and $b \sim \pm 8^\circ$ is known as Cygnus X region. *Right:* Finding chart for OB associations (circles) and young open clusters (asterisks) in the Cygnus region. For Cyg OB1 to Cyg OB9 only the OB numbers are quoted.

the mechanical power provided by Cyg OB2 (Comerón et al. 1998). In addition, the superbubble is equally well, if not even better, explained as a superposition of multiple objects at different distances that align along the local spiral arm that is seen tangentially in this direction (Bochkarev & Sitnik 1985; Uyaniker et al. 2001).

Also our cluster analysis seems difficult to reconcile with the scenario of an expanding bubble that triggered formation of the associations surrounding Cyg OB2. Firstly, the central association Cyg OB2 is one of the youngest in the area (1 – 4 Myr) while the surrounding associations Cyg OB1, OB3, OB7, and OB9 are slightly older (2 – 6 Myr). In the scenario where Cyg OB2 triggered the formation of the other associations, however, the situation should be vice versa. Secondly, only Cyg OB1 and OB3 are situated at distances that are compatible with that of Cyg OB2 while Cyg OB7 and OB9 are likely foreground objects. In addition, Cyg OB2 is not situated at the centre of the X-ray superbubble and the other OB associations correlate only partly with the structure (Uyaniker et al. 2001), making a physical relation of these objects highly questionable. Thirdly, the expansion age determined by Comerón et al. (1998) from stellar proper motions fits surprisingly well our age estimate for Cyg OB2, supporting the idea that the expanding stars are dynamically ejected runaway stars from Cyg OB2 (Comerón et al. 1998). Comerón et al.’s list of candidate members of the Cygnus expanding structure contains four O-type stars, which compared to the total of 120 O-type stars in Cyg OB2 (Knödseder 2000) would result in a runaway star fraction of 3% for this association. Compared to other young massive star associations, such as the Trapezium cluster in Orion or the λ Orionis star-forming region (Hoogerwerf et al. 2001), such a proportion seems typical, and we believe that at least part, if not all, of the anomalous stellar proper motions in Cygnus are indeed explained by runaway stars.

3.8. First estimates

Using simple approximations we can already make a first order estimate of the ionising flux that we expect from the stellar populations in the Cygnus region. The CoStar models of Schaerer & de Koter (1997) predict a Lyman continuum luminosity of $\log Q_0 = 49.05$ ph s^{-1} for a star of spectral type O7V, and assuming that all 204 O stars that we find in the associations of the Cygnus region are indeed O7V stars, we derive a total luminosity of $\log Q = 51.36$ ph s^{-1} . Assuming further that all stars lie at a typical distance of 1.8 kpc, and using the relation

$$S_{53} \text{ (Jy)} = 8.06 \times 10^{-48} \frac{Q}{s^2} \left(\frac{T_e}{8000 \text{ K}} \right)^{-0.45} \quad (4)$$

(s is the distance in units of kpc, Q is the Lyc luminosity given in ph s^{-1} , and T_e is the electron temperature which we assume to 8000 K; c.f. Afferbach et al. 1997) we predict a 53 GHz free-free emission flux of ~ 5700 Jy. We will see in the next section that this flux level is of the same order as the observed value.

4. Modelling the Cygnus region

4.1. Gamma-ray and microwave observations

Before we present the results of our evolutionary synthesis modelling we want to discuss the gamma-ray and microwave observations that triggered our investigation. Maps of 1.809 MeV gamma-ray line emission and 53 GHz free-free emission of the Cygnus regions are shown in superposition in Fig. 2. The spatial correlation between both emission features is striking. However, we want to caution the reader of overinterpretations of the apparent structures in the map. The gamma-ray feature has a total significance of only $\sim 8\sigma$, and the detailed morphology of the image is heavily biased by instrumental noise (Knödseder et al. 1999b). Formally, the COMPTEL instrument had

an angular resolution of $\sim 4^\circ$ (FWHM), yet the small amplitude of the signal probably does not allow inferences at angular scales below $\sim 10^\circ$. This is comparable to the angular resolution of 7° (FWHM) for the *COBE* DMR experiment which was used to derive the free-free emission map.

Observations of galactic radio-continuum emission from Cygnus at smaller angular scales indicate that most of the emission originates from a region between $l \sim 74^\circ$ and 84° with emission peaks around $l \sim 80^\circ$ (e.g. Wendker 1970). This region coincides with the OB associations Cyg OB1, Cyg OB2, Cyg OB8, and Cyg OB9 and a large number of the youngest open clusters in our database. However, the small-scale radio maps that are available were generally obtained at lower frequencies where synchrotron emission contributes significantly to the signal. Although the Cygnus emission is primarily optically thin thermal radiation, a superimposed smooth non-thermal component makes the determination of absolute free-free emission levels difficult (Wendker et al. 1991). Despite the poor angular resolution, we therefore prefer using the 53 GHz free-free emission map of Bennett et al. (1992) for the estimation of the ionising flux in Cygnus. At this frequency the contribution from synchrotron and thermal dust emission is small within the galactic plane, and can easily be removed by modelling their spatial distribution at adjacent frequencies. The image shown in Fig. 2 results from such a separation performed on DMR data (Bennett et al. 1992).

Smaller angular scales are probably even not desirable for a global flux comparison, although they bear valuable information about the interplay between the massive stars with the interstellar medium. Firstly, at angular scales that are smaller than the associations, the flux distribution may be influenced by individual massive stars, which we do not attempt to model in our study. Secondly, the correlation between free-free emission and the massive star distribution may anyway break-down at scales comparable to the association dimensions due to the lack of gas in their ploughed interiors. For example, Huchtmeier & Wendker (1977) did not find any H II region inside Cyg OB2 despite the large number of ionising stars that is present. They argue that the association is devoid of hydrogen and the ionising flux is converted into free-free emission by the surrounding gas, leading to a diffuse extended emission component. Thirdly, the long lifetime of ^{26}Al ($\tau \sim 1$ Myr) allows the isotope to travel substantial distances before the emission of the gamma-ray decay photons, and the detailed 1.809 MeV emission structure should depend considerably on the interaction and deceleration of the ejecta in the surrounding interstellar medium. Morphology studies that address the question of ejecta propagation in the Cygnus region will become possible with the upcoming *INTEGRAL* observatory (e.g. Knödlseeder & Vedrenne 2001), but the existing COMPTEL data limits our analysis to only a global investigation.

Table 4. Flux measurements and derived equivalent O7V star ^{26}Al yield of the Cygnus region. For comparison, the galactic average Y_{26}^{O7V} value is also quoted.

Quantity	Measured value
S_{1809}	$(5.8 \pm 1.5) \times 10^{-5} \text{ ph cm}^{-2}\text{s}^{-1}$
S_{1137}	-
S_{53}	$4200 \pm 700 \text{ Jy}$
Y_{26}^{O7V}	$(1.1 \pm 0.3) \times 10^{-4} M_\odot$
Y_{26}^{O7V} (Galaxy)	$(1.0 \pm 0.3) \times 10^{-4} M_\odot$

We determined the 1.809 MeV and 53 GHz free-free fluxes from the Cygnus region by integrating the respective skymaps over the area of interest. A diffuse galactic ridge emission that underlies the features in the Cygnus region has been subtracted from the flux estimates in order to extract the emission that is correlated to the Cygnus associations. The resulting flux estimates are only weakly sensitive on the precise location of the integration boundaries. To safely cover the investigated region we selected a longitude interval from $l = 65^\circ$ to 110° for the flux determination and determined the galactic ridge background from two adjacent intervals at $l = 110^\circ - 130^\circ$ and $l = 60^\circ - 65^\circ$. We selected a rather large latitude window of $|b| < 30^\circ$ to assure that we recover also the tails of the emission (in particular the COMPTEL skymap shows extended high latitude wings due to the low significance of the reconstructed emission). The resulting 1.809 MeV gamma-ray line flux amounts to $S_{1809} = (5.8 \pm 1.5) \times 10^{-5} \text{ ph cm}^{-2}\text{s}^{-1}$ while the 53 GHz free-free emission flux equals $S_{53} = 4200 \pm 700 \text{ Jy}$. The quoted errors reflect both the statistical and the systematical uncertainties in the flux determination, in particular those introduced by the selection of the integration boundaries.

The flux measurements can be converted into the equivalent O7V star ^{26}Al yield using

$$Y_{26}^{\text{O7V}} (M_\odot) = 7.91 \times 10^3 \frac{S_{1809} (\text{ph cm}^{-2}\text{s}^{-1})}{S_{53} (\text{Jy})}. \quad (5)$$

We obtain $Y_{26}^{\text{O7V}} = (1.1 \pm 0.3) \times 10^{-4} M_\odot$ for the Cygnus region, a value that is compatible with the galactic average value of $(1.0 \pm 0.3) \times 10^{-4} M_\odot$. The flux measurements are summarised together with the equivalent ^{26}Al yields in Table 4.

4.2. Evolutionary synthesis modelling

4.2.1. Prior probabilities and model uncertainties

We used the method described in Cerviño et al. (2000) and Sect. 2 to estimate the nucleosynthesis yields and Lyc luminosity for each association. The results are compiled in Tab. 5. For each association 100 statistically independent evolutionary synthesis models have been calculated to approximate the PDFs for all quantities of interest. Based on our age determinations, we marginalised the age

Table 5. Results of the evolutionary synthesis calculations. The quoted values are the medians of the posterior probability density functions, and the (asymmetric) errors specify the central 63.8% confidence intervals.

Name	$\log Y_{26}$ (M_{\odot})	$\log Y_{60}$ (M_{\odot})	$\log Q$ (ph s^{-1})	$\log S_{1809}$ ($\text{ph cm}^{-2}\text{s}^{-1}$)	$\log S_{1137}$ ($\text{ph cm}^{-2}\text{s}^{-1}$)	$\log S_{53}$ (Jy)	N_O	N_{WR}
Cep OB1a	$-3.2^{+0.2}_{-0.4}$	$-\infty$	$49.8^{+0.5}_{-0.4}$	$-6.3^{+0.3}_{-0.4}$	$-\infty$	$1.7^{+0.5}_{-0.4}$	$12.7^{+6.5}_{-12.7}$	$1.8^{+2.5}_{-1.7}$
Cep OB1b	$-4.3^{+0.3}_{-0.4}$	$-3.9^{+0.2}_{-0.3}$	$46.8^{+0.5}_{-0.5}$	$-7.3^{+0.4}_{-0.4}$	$-7.6^{+0.3}_{-0.3}$	$-1.4^{+0.5}_{-0.5}$	0	0
Cep OB2	$-4.8^{+0.5}_{-0.9}$	$-4.4^{+0.3}_{-0.5}$	$46.4^{+0.4}_{-0.4}$	$-6.3^{+0.5}_{-0.9}$	$-6.6^{+0.3}_{-0.5}$	$-0.3^{+0.4}_{-0.4}$	0	0
Cyg OB1	$-3.4^{+0.3}_{-0.3}$	$-3.8^{+0.5}_{-\infty}$	$49.6^{+0.5}_{-0.7}$	$-5.9^{+0.3}_{-0.4}$	$-7.0^{+0.5}_{-\infty}$	$2.0^{+0.6}_{-0.7}$	$5.6^{+8.7}_{-5.6}$	$1.0^{+2.3}_{-1.0}$
Cyg OB2	$-2.6^{+0.2}_{-1.0}$	$-\infty$	$51.0^{+0.2}_{-0.6}$	$-5.0^{+0.4}_{-1.0}$	$-\infty$	$3.5^{+0.3}_{-0.5}$	$97.1^{+18.7}_{-46.6}$	$8.9^{+8.9}_{-8.9}$
Cyg OB3	$-3.3^{+0.2}_{-0.4}$	$-\infty$	$49.9^{+0.5}_{-0.3}$	$-5.8^{+0.4}_{-0.5}$	$-\infty$	$2.2^{+0.5}_{-0.5}$	$12.4^{+7.9}_{-12.4}$	$1.9^{+2.5}_{-1.8}$
Cyg OB7	$-7.3^{+3.3}_{-\infty}$	$-\infty$	$48.7^{+0.6}_{-0.7}$	$-9.0^{+3.3}_{-\infty}$	$-\infty$	$1.8^{+0.6}_{-0.7}$	$0.4^{+1.8}_{-0.4}$	$0.0^{+0.3}$
Cyg OB8	$-4.0^{+0.3}_{-0.6}$	$-3.8^{+0.2}_{-\infty}$	$47.7^{+1.8}_{-1.1}$	$-6.6^{+0.4}_{-0.6}$	$-7.2^{+0.4}_{-\infty}$	$-0.1^{+1.8}_{-1.1}$	$0.0^{+5.7}$	$0.0^{+0.3}$
Cyg OB9	$-3.7^{+0.4}_{-1.2}$	$-\infty$	$49.4^{+0.5}_{-0.4}$	$-5.8^{+0.4}_{-1.2}$	$-\infty$	$2.1^{+0.5}_{-0.5}$	$4.4^{+2.7}_{-4.4}$	$0.3^{+1.4}_{-0.3}$
Lac OB1	$-4.5^{+0.3}_{-0.5}$	$-4.2^{+0.3}_{-0.4}$	$46.6^{+0.3}_{-0.2}$	$-6.0^{+0.4}_{-0.6}$	$-6.4^{+0.4}_{-0.4}$	$-0.1^{+0.3}_{-0.3}$	0	0
Vul OB1	$-4.2^{+0.5}_{-\infty}$	$-\infty$	$48.8^{+0.6}_{-0.7}$	$-6.9^{+0.5}_{-\infty}$	$-\infty$	$1.0^{+0.6}_{-0.7}$	$0.3^{+2.6}_{-0.3}$	$0.0^{+0.7}$
Berkeley 86	$-4.3^{+0.5}_{-\infty}$	$-\infty$	$48.7^{+0.5}_{-0.7}$	$-6.7^{+0.6}_{-\infty}$	$-\infty$	$1.2^{+0.5}_{-0.7}$	$0.1^{+1.9}_{-0.1}$	$0.0^{+0.6}$
Berkeley 87	$-3.9^{+0.4}_{-0.6}$	$-4.2^{+0.5}_{-\infty}$	$48.9^{+0.4}_{-0.7}$	$-6.4^{+0.6}_{-0.8}$	$-7.5^{+0.7}_{-\infty}$	$1.3^{+0.7}_{-0.7}$	$0.0^{+3.3}$	$0.0^{+1.0}$
Berkeley 94	$-\infty$	$-\infty$	$48.2^{+0.7}_{-2.0}$	$-\infty$	$-\infty$	$-0.4^{+0.7}_{-1.9}$	$0.0^{+0.8}$	$0.0^{+0.2}$
Berkeley 96	$-\infty$	$-\infty$	$47.2^{+0.9}_{-1.2}$	$-\infty$	$-\infty$	$-1.3^{+0.9}_{-1.2}$	0	0
Biukaran 2	$-6.6^{+1.3}_{-2.5}$	$-5.7^{+0.5}_{-1.0}$	$44.8^{+0.2}_{-0.2}$	$-9.2^{+1.3}_{-2.5}$	$-9.0^{+0.5}_{-1.0}$	$-2.9^{+0.3}_{-0.3}$	0	0
IC 4996	$-4.8^{+0.7}_{-\infty}$	$-4.8^{+0.7}_{-\infty}$	$47.6^{+0.8}_{-0.7}$	$-7.2^{+0.7}_{-\infty}$	$-7.9^{+0.7}_{-\infty}$	$0.1^{+0.8}_{-0.8}$	0	0
NGC 6823	$-4.1^{+0.6}_{-\infty}$	$-\infty$	$49.3^{+0.6}_{-0.6}$	$-6.9^{+0.7}_{-\infty}$	$-\infty$	$1.4^{+0.6}_{-0.7}$	$2.9^{+3.2}_{-2.9}$	$0.0^{+0.9}$
NGC 6871	$-4.2^{+0.3}_{-\infty}$	$-4.3^{+0.4}_{-\infty}$	$48.3^{+0.6}_{-0.5}$	$-6.9^{+0.4}_{-\infty}$	$-7.6^{+0.4}_{-\infty}$	$0.4^{+0.6}_{-0.6}$	0	$0.0^{+0.3}$
NGC 6883	$-4.9^{+0.4}_{-0.7}$	$-4.3^{+0.3}_{-0.6}$	$46.1^{+0.3}_{-0.6}$	$-7.3^{+0.5}_{-0.8}$	$-7.5^{+0.5}_{-0.6}$	$-1.5^{+0.5}_{-0.6}$	0	0
NGC 6910	$-7.1^{+3.1}_{-\infty}$	$-\infty$	$48.3^{+0.5}_{-0.9}$	$-9.6^{+3.2}_{-\infty}$	$-\infty$	$0.7^{+0.5}_{-0.9}$	$0.0^{+0.7}$	0
NGC 6913	$-4.8^{+1.1}_{-\infty}$	$-\infty$	$48.8^{+0.6}_{-0.7}$	$-7.3^{+1.3}_{-\infty}$	$-\infty$	$1.2^{+0.8}_{-0.8}$	$0.5^{+1.9}_{-0.5}$	$0.0^{+0.6}$
NGC 7067	$-4.7^{+0.3}_{-0.5}$	$-4.0^{+0.3}_{-0.4}$	$46.3^{+0.2}_{-0.2}$	$-8.2^{+0.3}_{-0.5}$	$-8.3^{+0.3}_{-0.4}$	$-2.4^{+0.2}_{-0.2}$	0	0
NGC 7128	$-5.5^{+0.6}_{-1.2}$	$-5.2^{+0.3}_{-0.5}$	$45.2^{+0.2}_{-0.2}$	$-8.6^{+0.6}_{-1.2}$	$-9.1^{+0.3}_{-0.5}$	$-3.2^{+0.3}_{-0.3}$	0	0
NGC 7160	$-5.4^{+0.9}_{-\infty}$	$-4.8^{+0.5}_{-\infty}$	$46.2^{+0.6}_{-1.1}$	$-7.3^{+0.9}_{-\infty}$	$-7.4^{+0.5}_{-\infty}$	$-0.9^{+0.6}_{-1.1}$	0	0
NGC 7235	$-3.8^{+0.3}_{-0.7}$	$-4.2^{+0.4}_{-\infty}$	$49.1^{+0.3}_{-0.4}$	$-6.9^{+0.4}_{-0.7}$	$-7.9^{+0.4}_{-\infty}$	$0.9^{+0.4}_{-0.5}$	$0.6^{+2.6}_{-0.6}$	$0.1^{+1.0}_{-0.1}$
NGC 7261	$-5.1^{+0.5}_{-1.2}$	$-4.6^{+0.4}_{-0.6}$	$46.0^{+0.4}_{-0.4}$	$-8.1^{+0.6}_{-1.2}$	$-8.3^{+0.5}_{-0.7}$	$-2.2^{+0.4}_{-0.4}$	0	0
NGC 7380	$-4.5^{+0.6}_{-\infty}$	$-5.7^{+1.5}_{-\infty}$	$48.3^{+0.6}_{-\infty}$	$-7.5^{+0.6}_{-\infty}$	$-9.4^{+1.5}_{-\infty}$	$0.1^{+0.6}_{-0.8}$	$0.0^{+0.7}$	$0.0^{+0.2}$
Roslund 4	$-4.9^{+0.6}_{-1.6}$	$-4.5^{+0.4}_{-1.0}$	$46.5^{+1.0}_{-0.6}$	$-7.7^{+0.7}_{-1.6}$	$-8.1^{+0.5}_{-1.0}$	$-1.4^{+1.0}_{-0.7}$	0	0
Roslund 5	$-8.5^{+2.7}_{-\infty}$	$-6.4^{+1.0}_{-2.7}$	$44.5^{+0.5}_{-1.0}$	$-9.8^{+2.7}_{-\infty}$	$-8.4^{+1.0}_{-2.8}$	$-2.0^{+0.5}_{-1.0}$	0	0
Ruprecht 175	$-\infty$	$-7.6^{+1.9}_{-\infty}$	$43.9^{+0.8}_{-1.9}$	$-\infty$	$-10.8^{+1.9}_{-\infty}$	$-\infty$	0	0
Trumpler 37	$-3.9^{+0.4}_{-0.6}$	$-4.2^{+0.5}_{-\infty}$	$49.0^{+0.4}_{-0.7}$	$-5.8^{+0.4}_{-0.6}$	$-6.9^{+0.5}_{-\infty}$	$1.8^{+0.5}_{-0.7}$	$0.0^{+3.5}$	$0.0^{+1.2}$
total	-	-	-	$-4.6^{+0.2}_{-0.2}$	$-5.7^{+0.3}_{-0.1}$	$3.7^{+0.2}_{-0.4}$	$145.1^{+26.5}_{-46.0}$	$22.6^{+10.9}_{-9.7}$

uncertainty using Eq. 1 with bounded Gaussian-shaped prior probability distributions. The mean and standard deviation of the Gaussians were defined by the mean and the half-width of the age boundaries quoted in column 2 of Tab. 2; the prior density was set to zero for ages outside the age boundaries. The ^{26}Al and ^{60}Fe yields as well as the Lyc luminosities that result from this procedure are given in columns 2 – 4 of Tab. 5.

Alternatively, we also tried box-shaped prior distributions that were bounded by our age estimates, but the results were only slightly different. In fact, Eq. 1 performs a weighted average of the PDFs where the age prior $p(t)$ defines the weights that are attributed to each age. From our association analysis we derive a possible range of ages, yet the data are not sufficiently accurate to derive details about the age distribution. Therefore, any prior distribu-

tion that reflects reasonably well the fact that the association age is comprised between two limits should provide a valid prior for our analysis. The only difference between the Gaussian and the box-shaped prior is that the first slightly favours models with an age close to the mean age between the boundaries, while the second gives equal weight to all ages that are compatible with the assigned limits. Since the observed age spread is at least partly due to measurement uncertainties, and since we defined our age boundaries as two extreme limits that enclose the age distribution of the most luminous stars, we feel that a bounded Gaussian-shaped prior reflects most properly the information that we have at hand about the association ages.

We also want to emphasise that our age marginalisation is equivalent to the assumption of a continuous star formation over an interval defined by the age boundaries. In this interpretation, the form of the age prior specifies the time evolution of the star formation rate. Since this rate is generally unknown, a rather flat prior distribution, like those we discussed above, is certainly appropriate. The interpretation of the apparent age distribution in the H-R diagram is usually a difficult enterprise due to the blending between measurement uncertainties, spectral misclassification, neglect of binarity and rotation, non-member pollution, and a possible non-coeval star formation. We cannot distinguish between all these uncertainties either, yet our formalism includes all of them into the model results.

The nucleosynthesis yields and ionising luminosity were converted into gamma-ray line and microwave free-free fluxes by marginalising the distance uncertainty for each association (Eq. 2). For the 1.809 MeV gamma-ray line flux due to the radioactive decay of ^{26}Al we used the relation

$$S_{1809} \text{ (ph cm}^{-2}\text{s}^{-1}\text{)} = 1.18 \times 10^{-2} \frac{Y_{26}}{s^2} \quad (6)$$

while for the 1.137 MeV gamma-ray line flux from the decay of ^{60}Fe we employed

$$S_{1137} \text{ (ph cm}^{-2}\text{s}^{-1}\text{)} = 2.41 \times 10^{-3} \frac{Y_{60}}{s^2} \quad (7)$$

(Y_{26} and Y_{60} are the ^{26}Al and ^{60}Fe yields in units of M_{\odot} , respectively, s is the distance in units of kpc). Note that the ^{60}Fe decay leads in fact to two gamma-ray lines at 1.137 and 1.332 MeV, but since their branching ratio and thus their intensity is basically identical we only quote the flux for the 1.137 MeV line. The conversion from ionising luminosity to 53 GHz free-free flux is given by Eq. 4. As distance priors $p(s)$ we used Gaussians with means and standard deviations that were defined by the distance moduli means and errors given in column 3 of Tab. 1. Again, since the distance modulus uncertainty arises primarily from measurement uncertainties, we believe that a Gaussian-shaped prior is a reasonable representation of our distance knowledge. The resulting 1.809 MeV, 1.137 MeV, and 53 GHz fluxes are quoted in columns 5 – 7 of Tab. 5.

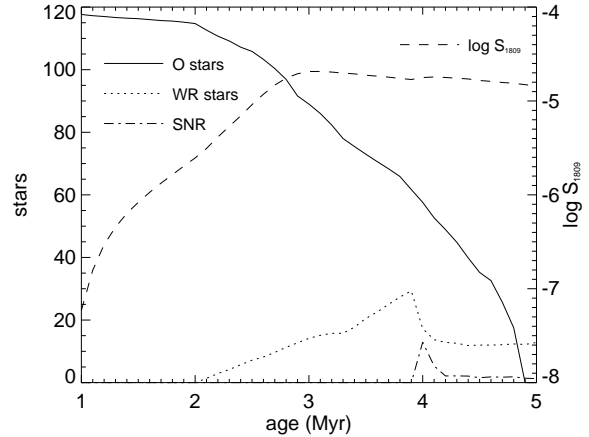


Fig. 3. Evolution of the number of O stars, Wolf-Rayet stars, supernova remnants, and 1.809 MeV gamma-ray line flux as function of age for Cyg OB2. We assumed a lifetime of 10^5 yr for each SNR.

Our evolutionary synthesis model also predicts the spectral type distribution, and we quote in columns 8 – 9 of Tab. 5 the predicted number of O-type and Wolf-Rayet stars. These predictions can be directly compared to the respective columns of Tab. 2, and we globally find a good agreement although the median values often fall below the observed values. The exception to the rule is Cyg OB2 for which the models predict between 51 and 116 O stars while the observations suggest 120. However, as discussed in Sect. 3.6, the 120 O stars quoted in Tab. 2 are rather an upper limit since the *2MASS* analysis did not account for possible evolutionary effects. Yet, Cyg OB2 houses evolved stars and even shows indications for non-coeval and ongoing star formation (e.g. Torres-Dodgen et al. 1991; Massey & Thompson 1991; Parthasarathy et al. 1992; Pigulski & Kolaczowski 1998; Herrero et al. 1999).

The effect of the age uncertainty on the stellar population in Cyg OB2 is illustrated in Fig. 3. For a coeval star formation event, the number of O stars drops rapidly from the initial value of 120 to zero during the first 5 Myr of the association evolution. Clearly, there is a considerable number of O-type stars in Cyg OB2 (e.g. Massey et al. 1991), hence the associations should be younger than 5 Myr. Wolf-Rayet stars appear around 2 Myr after the starburst while the first supernovae explode about 4 Myr after the birth of the association. The fact that there are Wolf-Rayet stars associated with Cyg OB2 suggests an age $\gtrsim 2$ Myr, the presence of 2 WC-type stars even indicates an age above 3 Myr. On the other hand no supernova remnant has been detected within the boundaries of Cyg OB2 (Wendker et al. 1991), hence the association should be younger than ~ 4 Myr. The 1.809 MeV gamma-ray line flux raises from zero to a maximum level of 2×10^{-5} ph cm $^{-2}$ s $^{-1}$ within ~ 3 Myr (for an assumed distance modulus of $DM = 11.0$ mag), and Cyg OB2 could be situated just at the maximum of the 1.809 MeV gamma-ray light curve, which is about a factor of two above the

median value quoted in Tab. 5. Nevertheless, the present reasoning only holds for a strictly coeval star formation event, and the evidence for ongoing star formation in Cyg OB2 holds against narrowing down the age boundaries for the association. Clearly, more observational data is required to improve our knowledge about the age distribution in Cyg OB2 before we safely can improve upon the nucleosynthesis yield estimation for this association.

This example illustrates that the apparent age spread in the HRDs presents an important source of uncertainty for the final flux estimates, at least for the youngest associations. In general, however, the dominating source of uncertainty depends on the association richness and its age, but also on the nature of the quantity of interest. For Cyg OB2, for example, the 53 GHz flux prediction is much less affected by the age uncertainty than the 1.809 MeV flux estimate. While the 1.809 MeV flux varies by more than two magnitudes between 1 – 4 Myr, the number of O stars changes only by a factor of two, implying a 53 GHz flux variation by a factor of less than six. For slightly older associations, such as Trumpler 37, the situation is reversed: the 1.809 MeV flux varies only slowly while the ionising flux now drops quickly due to the disappearing of the most massive stars in supernovae events.

If the association is sufficiently rich so that sampling effects are negligible, the distance uncertainty turns out to be the dominating factor of the flux dispersion. Typically, the relative distance uncertainty for an association amounts to 20% which directly translates into a flux uncertainty of 40%. Sampling effects are important when only few stars contribute to the association luminosities, i.e. either for very young or for very poor populations. Cyg OB7 fulfils both conditions. For this association, a considerable fraction of the evolutionary synthesis samples did not lead to any ^{26}Al production at all. In those cases, the initial mass function has not been populated by sufficiently massive stars to lead to a noticeable ^{26}Al production during the conceivable age range of Cyg OB7 (2 – 5 Myr). We indicate such a possibility by quoting infinite negative errors in Tab. 5.

4.2.2. Correlated emission

To investigate the correlation between gamma-ray line flux and free-free emission in the Cygnus region we plotted the predicted 1.809 and 1.137 MeV fluxes versus the 53 GHz flux (Fig. 4). All three quantities should scale with distance and association richness, and indeed we find a general trend of increasing gamma-ray intensity with increasing free-free flux. A few associations with low gamma-ray fluxes ($\log S_{1809,1137} \approx -9$) deviate from this tendency, yet they represent those poorly populated clusters that show a tremendous flux dispersion due to poor sampling of the high-mass IMF (see above). To illustrate the distance and richness impact, we superimposed an arrow in Fig. 4 that indicates the displacement due to a decrease of

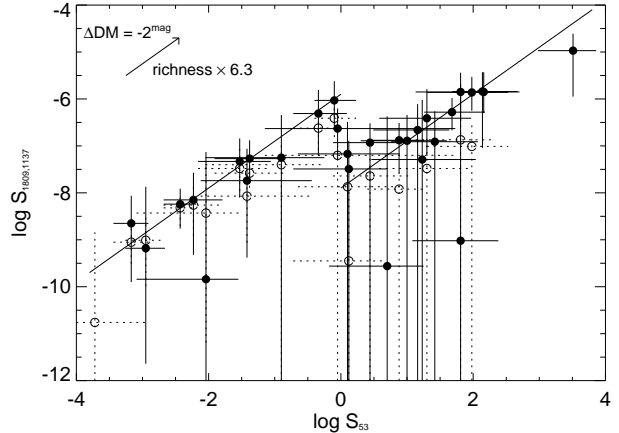


Fig. 4. Predicted 1.809 MeV (filled dots and solid error bars) and 1.137 MeV gamma-ray line fluxes (open dots and dashed error bars) as function of predicted 53 GHz free-free flux. The arrow indicates the displacement due to a decrease of 2 mag in the distance modulus or an increase of the richness by a factor of 6.3. The two solid lines indicate equivalent ^{26}Al O7V star yields of $\log Y_{26}^{\text{O7V}} = -2$ (left) and -4 (right).

2 mag in the distance modulus or an equivalent increase of the association richness by a factor of 6.3.

For the 1.809 MeV flux, the associations are situated along this line of displacement, yet there occurs a clear discontinuity around $\log S_{53} \approx 0$. All associations with $\log S_{53} < 0$ are older than 10 Myr, an evolutionary phase during which ^{26}Al is exclusively ejected by supernovae events (the only exception to this rule are Berkeley 94 and 96, yet they are so sparsely populated that no ^{26}Al production is expected). In contrast, all associations with $\log S_{53} > 0$ are younger than 10 Myr, hence they are dominated by ^{26}Al ejection through stellar winds (Cerviño et al. 2000). The discontinuity in Fig. 4 represents a change in the equivalent O7V star ^{26}Al yield, and we find typical values of $\log Y_{26}^{\text{O7V}} \approx -2$ and -4 for $\log S_{53} < 0$ and > 0 , respectively.

The discontinuity in the correlation coefficient may eventually lead to a break-down in the tight correlation between 1.809 MeV and 53 GHz emission, which should occur however at rather low 1.809 MeV flux levels of about 10^{-6} ph cm $^{-2}$ s $^{-1}$. At this level, it is expected to find 1.809 MeV emission features that are uncorrelated to microwave free-free emission (or for which the free-free emission should not exceed an intensity of 1 Jy). Given the sensitivity limit of the spectrometer SPI on *INTEGRAL*, it is unlikely that this break-down will be observable in the near future.

For the 1.137 MeV flux we find only a weak correlation with free-free emission, which is mainly limited to $\log S_{53} < 0$, i.e. older associations that are dominated by supernova explosions. For those, a typical equivalent O7V star ^{60}Fe yield of $\log Y_{60}^{\text{O7V}} \approx -1.5$ is found, yet the low

level of the associated free-free flux ($S_{53} < 1$ Jy) will inhibit the observation of this correlation. For $\log S_{53} > 0$, 1.137 MeV fluxes are highly uncertain due to the small number of supernova events that contribute to ^{60}Fe production (recall that no large amounts of wind-ejected ^{60}Fe is expected from massive stars; see Cerviño et al. 2000). The youngest associations, such as Cyg OB2 or Cyg OB3, show no ^{60}Fe production at all, despite the huge amounts of ionising photons that is produced by their large number of O-type stars.

By far the most luminous association in both 1.809 MeV and 53 GHz free-free emission is Cyg OB2, which corresponds to the isolated dot in the upper-right corner of Fig. 4. The median equivalent yield of Cyg OB2 amounts to $Y_{26}^{\text{O7V}} = 2.2 \times 10^{-5} M_{\odot}$, somewhat lower than the observed value of $1.1 \times 10^{-4} M_{\odot}$ in the Cygnus region. In other words, Cyg OB2 seems to underproduce ^{26}Al with respect to ionising photons, which is mainly related to its extremely young age. Most of the massive stars are still on the main sequence where they produce large amounts of ionising photons, but do not yet eject copious amounts of ^{26}Al in the interstellar medium.

For the entire Cygnus region, we find an equivalent O7V star ^{26}Al yield of $Y_{26}^{\text{O7V}} = 4.7 \times 10^{-5} M_{\odot}$, about a factor of two below the observed value. Apparently, our model underpredicts ^{26}Al production with respect to the ionising luminosity by about a factor of 2, and we will suggest later that this underprediction is most likely related to shortcomings of current nucleosynthesis models for massive stars. It is interesting to note that our predicted Y_{26}^{O7V} value is very close to the steady-state value of $4.9 \times 10^{-5} M_{\odot}$, which results for a stellar population with a constant star formation rate (Cerviño et al. 2000). Since the Cygnus region is largely dominated by a single association, Cyg OB2, we believe that this finding is merely a coincidence. Indeed, our predicted equivalent O7V star ^{60}Fe yield of $Y_{60}^{\text{O7V}} = 2.0 \times 10^{-5} M_{\odot}$ for the entire Cygnus region falls more than a factor of two below the steady-state value of $5.6 \times 10^{-5} M_{\odot}$ (Cerviño et al. 2000), emphasising the relative rareness of supernova events in the Cygnus region with respect to a steady-state population.

4.2.3. Spatial distribution

To illustrate the spatial distribution of the 1.809 MeV and 53 GHz emission predicted by our model, we show in Fig. 5 intensity maps for both observables that are based on the median flux values quoted in Tab. 5. Although we have no information about the spatial distribution of the respective emission within and around the associations, we distributed the flux within the association boundaries using Gaussian-shaped density profiles to account for the spatial extent of the stellar populations. We recall that the true distribution could be more widespread due to the possible lack of ionised gas in the ploughed cluster interiors and the propagation of the radioactive ejecta before decay (cf. Sect. 4.1). In addition, when comparing these

distributions to the observed maps in Fig. 2, the angular resolution of the telescopes of 4° (COMPTEL) and 7° (DMR) has to be considered.

Taking these factors into account, the morphological resemblance of our model maps to the observations is quite reasonable. We predict free-free and 1.809 MeV emission maxima at $(l, b) \sim (80^{\circ}, 1^{\circ})$ which spatially coincides with the observed maximum of the 53 GHz map, and is also close the maxima in the 1.809 MeV COMPTEL map. The observations show copious emission in the longitude range $l \sim 70^{\circ} - 90^{\circ}$, and also our model predicts the bulk emission in this region. Obviously, the most prolific sources of 1.809 MeV and 53 GHz emission are (in the quoted order) the OB associations Cyg OB2, Cyg OB3, Cyg OB9, and Cyg OB1 that form the core of the Cygnus X complex (see Fig. 2). Cyg OB2 is by far the most important source in the area for which we predict median fluxes of $S_{1809} = 1 \times 10^{-5} \text{ ph cm}^{-2}\text{s}^{-1}$ and $S_{53} = 3200$ Jy. Comparison of the median values with the observed fluxes from the entire region (cf. Sect. 4.1) suggests that Cyg OB2 alone could provide around 75% of the ionisation in Cygnus while it may account for only $\sim 20\%$ of the observed 1.809 MeV photons. Including both observational and modelling uncertainties weakens this discrepancy, yet the general trend remains: within the uncertainties, Cyg OB2 could easily explain all ionisation in Cygnus while it can account at most for 60% of the observed ^{26}Al .

Using successive marginalisation (Eq. 3) we estimate the total flux from the associations and clusters in the Cygnus X area ($70^{\circ} \leq l \leq 82^{\circ}$; $-3^{\circ} \leq b \leq 6^{\circ}$) to $S_{1809} = (2.0_{-1.1}^{+1.6}) \times 10^{-5} \text{ ph cm}^{-2}\text{s}^{-1}$, $S_{1137} = (3.4_{-2.6}^{+6.1}) \times 10^{-8} \text{ ph cm}^{-2}\text{s}^{-1}$, and $S_{53} = 4000_{-2300}^{+3700}$ Jy. The ionising flux is in comfortable agreement with the integrated 53 GHz emission from the Cygnus region, while the 1.809 MeV flux falls significantly below the observed value. The predicted 1.137 MeV flux is way below the detection limit of any envisagable gamma-ray telescope, reflecting the extreme rareness of supernova events in this area. Stellar-wind ejection seems to dominate the enrichment of the interstellar medium by nucleosynthesis products in the Cygnus X region – more than 85% of the 1.809 MeV flux in our model originates from ^{26}Al that is ejected through this channel.

The second feature in the model map is low-level 1.809 MeV and 53 GHz free-free emission from some open clusters in the Cepheus region, in particular from Trumpler 37. Trumpler 37 is a young, rich, and nearby open cluster that is embedded into the bright H II region IC 1396. Distance estimates based on *Hipparcos* data vary between $DM = 9.1$ and 9.9 mag (de Zeeuw et al. 1999; Robichon et al. 1999) while our analysis results in a value of 10.2 ± 0.4 mag. Using this larger estimate we predict a median 1.809 MeV flux of $1.6 \times 10^{-6} \text{ ph cm}^{-2}\text{s}^{-1}$. Adopting the short *Hipparcos* distance of de Zeeuw et al. (1999) would result in a flux of $S_{1809} = 3.9 \times 10^{-6} \text{ ph cm}^{-2}\text{s}^{-1}$, making Trumpler 37 a potential source of 1.809 MeV γ -ray line emission in an area that is little affected by source con-

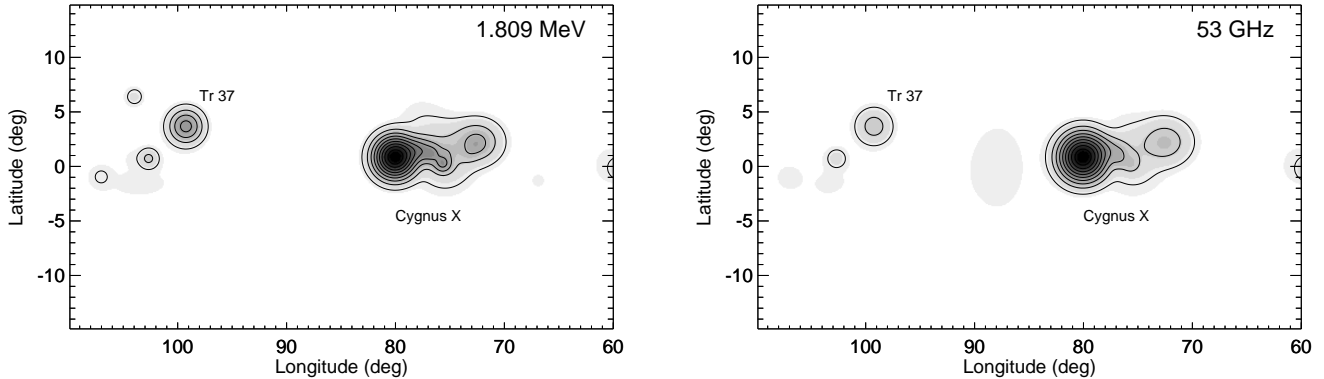


Fig. 5. Predicted median 1.809 MeV gamma-ray line intensity distribution (left) and 53 GHz microwave free-free intensity (right).

fusion. COMPTEL observations (cf. Fig. 2) do not show any feature in this area, yet the predicted flux is considerably below the sensitivity limit of this instrument. With its improved sensitivity, the SPI telescope aboard the upcoming *INTEGRAL* observatory may be able to detect this emission, in particular if current nucleosynthesis models indeed underestimate ^{26}Al production in massive stars (see below).

4.2.4. Integrated emission

Finally, the luminosities of all associations have been combined by successive marginalisation (Eq. 3) to predict the total fluxes from the Cygnus region; the results are presented in the last row of Tab. 5. For the entire Cygnus region we obtain a median 53 GHz flux of 5000 Jy, close to the observed value of 4200 ± 700 Jy. The total predicted 1.809 MeV flux, however, is significantly below the observations: while the model predicts a median gamma-ray line flux of $S_{1809} = 2.5 \times 10^{-5}$ ph cm $^{-2}$ s $^{-1}$ and a 63.8% confidence interval of $(1.6 - 4.0) \times 10^{-5}$ ph cm $^{-2}$ s $^{-1}$, the COMPTEL data suggest a value of $(5.8 \pm 1.5) \times 10^{-5}$ ph cm $^{-2}$ s $^{-1}$. Our model predicts only little ^{60}Fe synthesis in Cygnus, and consequently, the predicted median 1.137 MeV flux amounts to only $S_{1137} = 2 \times 10^{-6}$ ph cm $^{-2}$ s $^{-1}$. At this level, it seems unlikely that the SPI telescope will detect the radioactive decay of the ^{60}Fe isotope in the Cygnus region.

On average, about 80% of the 1.809 MeV emission in our model originates from ^{26}Al ejected by stellar winds while only 20% come from core-collapse supernovae. Also, OB associations play a dominant role in the Cygnus region since they contribute to almost 80% of the 1.809 MeV emission and to about 90% of the free-free luminosity.

Our model predicts 99 – 172 O stars and 13 – 34 Wolf-Rayet stars in the Cygnus region associations, about $\sim 25\%$ less than we find in our cluster database. We think that this discrepancy is acceptable, in particular in view of the strong variation of the O star number with association age (Fig. 3). Note that in any case, the missing O stars

cannot explain the apparent underestimation of the 1.809 MeV luminosity, since lowering the age estimates of some associations (in particular Cyg OB2) to increase the number of O stars tends also to lower the ^{26}Al production. On the other hand, an important increase in the number of O stars will also increase proportionally the ionising flux for the Cygnus region, leading quickly to an overproduction of Lyc photons.

5. Discussion

One essential finding from a census of all known clusters and OB associations and our modelling effort is that we can comfortably reproduce the ionising flux from the Cygnus region, while we fall short by a factor of 2 in explaining ^{26}Al nucleosynthesis. There are two possibilities that may lead to such a result: either the nucleosynthesis models we employed underpredict ^{26}Al production by about a factor of 2, or we overpredict the ionising flux by about a factor of 2, and in the same time, underestimate the stellar population in the Cygnus region by about the same factor. We tend to believe that the problem is more likely related to the nucleosynthesis models, and in the following we will present the elements that lead us to this conclusion.

5.1. Ionisation

Our prediction of the ionising flux from the Cygnus region relies on stellar atmosphere models that predict the stellar Lyman continuum luminosities as function of the stellar parameters. However, the lack of spectroscopic data in the extreme ultraviolet shortward of the hydrogen ionisation limit leaves these models basically untested in this wavelength region, and we have to consider the reliability of the employed atmosphere models in predicting Lyc fluxes.

The status of predictions of ionising fluxes has recently been reviewed by Schaerer (1998, 1999). From a comparison of Lyman continuum photon fluxes predicted by various atmospheric models, Vacca et al. (1996)

concluded that they are consistent to within 20%. Oey & Kennicutt (1997) compared observed H II region luminosities in the Large Magellanic Cloud to the Lyman continuum luminosities predicted from their well-determined stellar content, using the CoStar atmosphere models of Schaerer & de Koter (1997) that we also employed in this work. They find that on average, H II region luminosities amount to 74% of the ionising luminosities predicted by the stellar models, leaving room for about 25% flux overprediction by the models. Hunter & Massey (1990) come to a similar conclusion, using the stellar Lyc estimates of Panagia (1973) applied to small galactic H II regions. However, accounting for the downward revision of the effective temperature scale due to non-LTE line blanketing effects, reduces the Lyc fluxes for a given spectral type (Martins et al. 2002) eliminating the overprediction found by the above studies.

On the other hand, it is commonly believed that some fraction of the ionising photons escape the H II regions and ionise the diffuse, warm, ionised medium (WIM) of the Galaxy (e.g. Oey & Kennicutt 1998). The WIM has been found to comprise 20 – 53% of the total H α luminosity in nearby star-forming galaxies (see Ferguson et al. 1996), a number that is consistent with the $\sim 25\%$ of ionising photons that are on average missing in the H II regions with respect to the model predictions. Our study is not much affected by the fraction of ionising photons escaping into the WIM, since our microwave flux estimate from the Cygnus region has been obtained by integrating over a rather larger spatial area, including both individual H II regions and the WIM (see Sect. 4.1).

Alternatively, ionising photons may be also absorbed by dust within the H II regions, and a recent study of Inoue et al. (2001) indicates that $\sim 20\%$ of the photons may be lost in small galactic H II regions in this way. Using a decomposition of DIRBE far-infrared data, Sodroski et al. (1997) estimated an infrared excess of 1.1–1.7, corresponding to 5% – 12% of Lyc photon absorption within the Galaxy (Mezger et al. 1974). Thus instead of ionising the WIM, the apparent 25% flux overprediction may be also (partly) explained by dust absorption.

Whatever the mechanism, 25% ionising flux overprediction by our model should be a rather solid upper limit, which is in any case far from the required factor of 2 that is needed to explain the ^{26}Al nucleosynthesis.

5.2. Completeness

In our aim to predict absolute fluxes from the OB associations and young open clusters in Cygnus, we have to be concerned about the completeness of our database. First, there might be more OB associations in Cygnus than those we listed in Table 1. Due to their extent and weak clustering, OB associations are generally difficult to identify, in particular if they are nearby. To estimate the association completeness, we compared the number of O stars in the Cygnus area from the SIMBAD database to the

number of O stars in our stellar database. Many entries in the SIMBAD database originate from the O star catalogue of Garmany et al. (1982), which is complete down to a visible magnitude of $V = 10$ mag, corresponding to a maximum $DM + A_V = 14.3$ mag for O type stars. Comparison of this limit to the distance moduli and reddenings in Table 1 shows that, except for Cyg OB2 and some of the heavily reddened or distant open clusters, the SIMBAD data should indeed be complete for the Cygnus region.

In total we find 171 MK classified O stars in the surveyed area in the SIMBAD database while our association database contains 204 O stars. Our excess in O stars is due to the 120 objects in the heavily reddened Cyg OB2 association that are only partially identified in SIMBAD (about 50%). Excluding Cyg OB2 from SIMBAD and our database results in 108 O stars in SIMBAD versus 84 O stars in our database, resulting in a completeness of almost 80%. Adding the 120 O stars of Cyg OB2 to both samples increases the O star completeness to about 90%. Thus, most known O stars are indeed located in the OB associations of our database.

Secondly, there may be young open clusters in Cygnus that escaped so far detection due to the heavy obscuration in this area. Indeed, using *2MASS* near-infrared data, Dutra & Bica (2001) found 21 new cluster candidates in our survey region ($60^\circ < l < 110^\circ$), which doubles the number of young open clusters in this area. Also, on basis of *2MASS* data, Le Duigou & Knödseder (2002) determined the stellar content of 15 new infrared cluster candidates in the area, and concluded that they triple the OB population with respect to the known open clusters in the centre of the Cygnus X region. However, compared to the giant association Cyg OB2, they contribute only a small fraction, and we find only an additional 10% of OB stars in the newly discovered clusters candidates.

Thus, in summary, we believe that our database is fairly complete, within about 10 – 20%, and that the 1.809 MeV luminosity puzzle can not be explained by a hidden population of massive stars. In any case, if there would be such a hidden population, it should also produce a considerable amount of ionising photons, which would lead quickly to an overproduction with respect to the microwave observations.

5.3. Rotation

Throughout this work we have ignored the effects of stellar rotation, mainly because there is not sufficient stellar data available for the stellar associations we are interested in, and since there are no stellar grids available so far that allow for inclusion of rotation in evolutionary synthesis calculations. Rotation firstly affects the colour and luminosity of a star, hence it may introduce an artificial age spread in the cluster HRDs (e.g. de Geus 1990; Lamers et al. 1997). Since we accounted for age uncertainties in our approach, however, we do not believe that neglecting

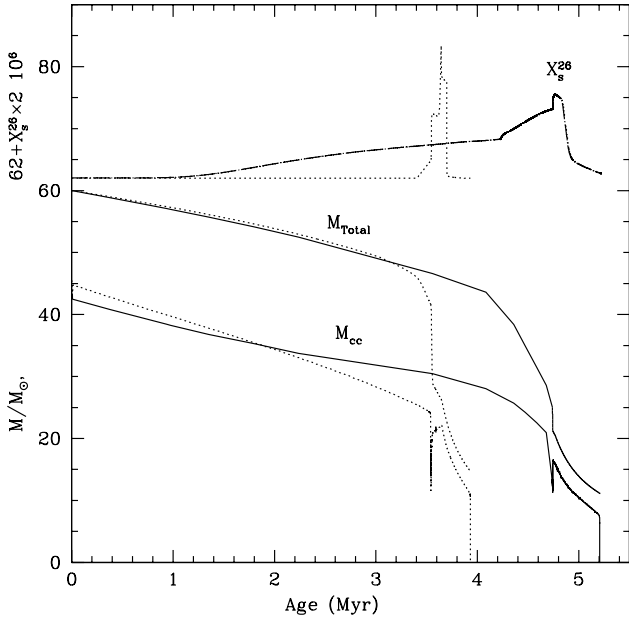


Fig. 6. Evolution as a function of time of the total mass of the star, M_{Total} , of the mass of the convective core, M_{cc} and of the surface abundance of ^{26}Al in mass fraction, X_s^{26} , for a rotating (continuous lines) and a non-rotating (dotted lines) $60 M_{\odot}$ stellar model at solar metallicity. The initial equatorial velocity for the rotating model is 300 km s^{-1} .

of rotation in the determination of the cluster parameters plays an important role.

Much more important may be the impact of rotation on stellar evolution and in particular the nucleosynthesis of ^{26}Al . To illustrate this point, we show in Fig. 6 the evolution of the surface ^{26}Al abundance as a function of time for two $60 M_{\odot}$ stellar models at solar metallicity with and without rotation (Ringger 2000). The models were computed with the same physical ingredients as used in Meynet & Maeder (2000). Let us note in particular that the mass-loss rates used by Ringger (2000) are smaller by a factor of 2–3 than the mass-loss rates used in the stellar models that have been applied to calculate the ^{26}Al yields in this work.

In the case of the rotating models, surface enrichments begin to occur at a much earlier stage than in the non-rotating model (see Fig. 6). Indeed rotational mixing brings freshly synthesised ^{26}Al at the surface well before shells, having experienced CNO processing, are uncovered by the stellar winds. This explains why the ^{26}Al abundance at the surface of the rotating model increases in a much smoother way than at the surface of the non-rotating model. One can see also that rotational mixing slows down the decrease in mass of the convective core and increases the Main Sequence lifetime. This results from the diffusion of hydrogen into the convective core. Some ^{25}Mg will also migrate from the radiative envelope into the convective core where it will be transformed into ^{26}Al . These effects

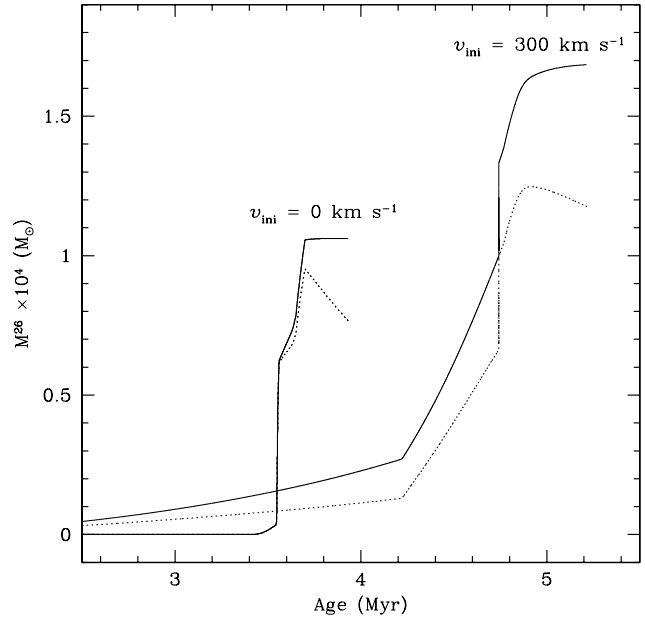


Fig. 7. Continuous lines show the evolution as a function of time of the integrated mass of ^{26}Al ejected by stellar winds for a non-rotating and a rotating $60 M_{\odot}$ stellar model at solar metallicity. The initial equatorial velocities are indicated. The dotted lines show the evolution of the mass of non-decayed ^{26}Al .

tend to increase the quantity of ^{26}Al ejected by the stellar winds.

Fig. 7 shows the evolution of M^{26} , the integrated mass of ^{26}Al ejected by the stellar winds by the rotating and non-rotating $60 M_{\odot}$ models. This quantity is obtained by estimating the integral

$$M^{26}(t) = \int_0^t X_s^{26}(t') \dot{M}(t') dt', \quad (8)$$

where \dot{M} is the mass loss rate. The luminosity at 1.809 MeV is, at each time, proportional to the mass of non-decayed ^{26}Al (see the dotted lines in Fig. 7). One sees that the maximum luminosity reached by the rotating model is shifted towards later time and is only slightly increased with respect to the non-rotating model. This occurs because in the rotating model, the release of the ^{26}Al is distributed over a much longer time, and therefore, the radionuclide has more time to decay. Thus even if the quantity of ^{26}Al released by the rotating model is significantly greater (for this particular model the enhancement factor is ~ 1.6), the enhancement of the luminosity is not as great. The above examples show that rotation, all other physical ingredients being kept equal, tends to increase the total quantity of ^{26}Al ejected, slightly increases the maximum 1.809 MeV luminosity, and shifts the ejection of the bulk of ^{26}Al to later times.

How the results of the present population synthesis models would be affected by rotation? First of all, let us

recall that the WR stellar models used in the present population synthesis models implicitly account in some way for non-standard physical mechanisms. Indeed these models were computed with artificially enhanced mass loss rates which enabled to account in a satisfactorily manner for the variation with the metallicity of the number of WR to O-type stars (Maeder & Meynet 1994). Thus the reproduction of this observational constraints in some way calibrates these stellar models. If we compare the total quantity of ^{26}Al ejected by our rotating $60 M_{\odot}$ model with the non-rotating $60 M_{\odot}$ model with enhanced mass loss rates, used in the present population synthesis model, we find a modest ^{26}Al yield increase of 13%.

Does this mean that rotation has to be discarded as a possible mechanism for solving the ^{26}Al deficit discussed in the present paper? We think it is too early to reach such a conclusion. Since the work of Ringger (2000), new improvements of the physics of rotation have been achieved especially concerning the shear diffusion coefficient and the impact of rotation on the mass loss rates (Maeder & Meynet 2000, 2001). Predictions of precise enhancement factors requires the computation of stellar models for different initial masses and rotational velocities. At the present time, no such grids of models, predicting the 1.809 MeV luminosity, have been computed. We therefore defer a more quantitatively assessment of rotation on gamma-ray line emission in Cygnus to future work.

5.4. Binarity

Binarity may be another mechanism that could alter the ^{26}Al yields from massive stars, yet we did not account for their effects due to the involved complexity and poorly known details. In particular, only close binary systems are concerned, and there is not sufficient data available for the associations we are interested in to assess their number and mass distribution.

Two effects may impact the nucleosynthesis in close binary systems: tidal interactions in close binary systems, and mass transfer by Roche Lobe overflow. Tidal effects are expected to deform the star and therefore induce instabilities reminiscent of those induced by rotation. In particular, tidal forces and orbital motions will induce rotation even in initially non-rotating stars. To our knowledge, this effect has never been studied in nucleosynthesis calculations, despite its potentially important consequences, as for instance by homogenising the stars.

If mass transfer occurs, the removal of part of the envelope of the donor star may favour the appearance of ^{26}Al on the surface, in a similar fashion as mass-loss acts through stellar winds. More important changes may occur for the gainer in systems with $M < 40M_{\odot}$, as e.g. shown by the preliminary studies of Braun & Langer (1995) and Langer et al. (1998). The latter suggest a scenario in which mass transfer onto the secondary leads to a rejuvenation which alters its subsequent evolution. They predict an increase by 2 – 3 orders of magnitudes of the hydro-

statically produced ^{26}Al yield due to a reduction of the delay between production and ejection of ^{26}Al , which may possibly enhance the total ^{26}Al production from Type II supernovae by a factor of about 2 (Langer, priv. communication). Since, however, supernovae are very rare in Cygnus, it is highly doubtful that such a mechanism could solve the ^{26}Al yield puzzle.

6. Conclusions

6.1. Nucleosynthesis

Our modelling effort of the gamma-ray line emission from OB associations and young open clusters in the Cygnus region has revealed a possible shortcoming of actual nucleosynthesis models in explaining ^{26}Al production. We find a 1.809 MeV flux underestimation of about a factor of 2 that is difficult to explain by other means than a modification of current nucleosynthesis models for single, non-rotating stars. From preliminary calculations, it appears difficult for rotation alone to significantly enhance ^{26}Al production, although this conclusion needs to be checked by more detailed calculations in the future.

Only little ^{60}Fe production is predicted in Cygnus by our model, mainly related to the low number of recent supernova events in this region. A detection of the 1.137 MeV and 1.332 MeV lines from the radioactive decay of ^{60}Fe by *INTEGRAL* would therefore present a big surprise. In the case of such a detection, ^{60}Fe production by hydrostatic helium burning in Wolf-Rayet stars – which we have not included in our model due to the low yield predictions – should then be seriously reconsidered (Arnould et al. 1997).

6.2. Other gamma-ray signatures

In addition to ^{26}Al and ^{60}Fe , massive star associations may produce further radioactive isotopes during the supernova explosion of massive stars, such as ^{56}Co and ^{44}Ti , yet their short lifetimes of 112 days and 87 years, respectively, make their observation impossible in absence of a very recent event. However, ^{56}Co and ^{44}Ti decay under positron emission (like ^{26}Al), and the annihilation of positrons with electrons of the interstellar medium on time scales of a few 10^5 years may provide a reverberation of the short-lived, extinct, radioactivities. Hence, the observation of the 511 keV positron annihilation line may provide an independent measure of the supernova activity in massive star associations (and in particular in Cygnus), although the interpretation of the observations will be complicated by the annihilation physics, the positron transport, and the positron escape fraction from the expanding supernova remnants.

6.3. Super star clusters

Gamma-ray as well as free-free emission in the Cygnus region seems to be dominated by a single, extremely massive

association: Cyg OB2. Indeed, Cyg OB2 is merely a prototype of a young globular cluster than an OB association (Knödseder 2000). There are examples of further super star clusters in the Galaxy, such as NGC 3603 (Moffat et al. 1994), the Arches and Quintuplet clusters near the galactic centre (Figer et al. 1999), or the W49A cluster (Conti & Blum 2002). Most of these super star clusters are partially or totally obscured in the visible by the absorbing effects of intervening and/or local interstellar dust, and it is unclear how many of them exist throughout the entire Galaxy. Making the simplifying assumption that super star clusters are distributed uniformly throughout the Galaxy within a galactocentric distance of 15 kpc, and taking that Cyg OB2 is apparently the only such object within 1.5 kpc, one may expect 100 super star clusters in our Galaxy. Assuming that they all produce $10^{-2} M_{\odot}$ of ^{26}Al , similar to our Cyg OB2 model prediction, a total ^{26}Al production of $1 M_{\odot}$ is expected from these objects. Taking into account the ^{26}Al yield underestimation of a factor of 2 brings this mass to $2 M_{\odot}$, comparable to the observed galactic ^{26}Al mass of $2 - 3 M_{\odot}$ (Diehl et al. 1995; Knödseder 1999). Thus, a considerable fraction of ^{26}Al maybe indeed produced by such super star clusters, and 1.809 MeV gamma-ray observations with sufficient angular resolution and sensitivity may help to uncover and to study them throughout the Milky-Way.

6.4. The Cygnus superbubble

Our age determination of clusters in the Cygnus region sheds some doubt on the triggered star formation scenario that has been proposed to explain anomalous stellar proper motions in the area (Comerón & Torra 1994). In this scenario, the central association Cyg OB2 is supposed of having formed a shell blown by stellar winds and supernovae, the Cygnus superbubble, that subsequently gave birth to the surrounding associations Cyg OB1, OB3, OB7 and OB9 due to gravitational shell instability. However, our age estimate for Cyg OB2 is inferior to that of the surrounding associations, making triggered star formation in this area unlikely. In contrast, the anomalous stellar proper motions are equally well explained by supposing that they result from dynamically ejected runaway stars from Cyg OB2 (Comerón et al. 1998), in particular since the proposed expansion age of ~ 4 Myr is compatible with our age estimate for Cyg OB2.

6.5. Cygnus and the Galaxy

Finally, we want to mention that not only the Cygnus region but also the Galaxy as a whole suffers probably from an underproduction of ^{26}Al when current, non-rotating nucleosynthesis models are considered. By combining the same nucleosynthesis models that have been used in this work with the atmosphere models of Schaerer & de Koter (1997), and normalisation to the observed galactic Lyman continuum luminosity,

Knödseder (1999) predicted a galactic ^{26}Al mass of $1.6 M_{\odot}$, significantly below the observed value of $2 - 3 M_{\odot}$. Only the inclusion of the galactic metallicity gradient, which considerably enhances ^{26}Al ejection through stellar winds in the Wolf-Rayet phase towards the galactic centre, provides a sufficient increase of the galactic ^{26}Al production, bringing the model predictions in better agreement with the observations.

Yet, metallicity is of no help in the Cygnus region, where even slightly subsolar abundances are reported (Daffon et al. 2001). On the other hand, if another process, such as rotation, is needed to explain the ^{26}Al production in Cygnus, it should also be at work for the entire Galaxy, leading to a potential ^{26}Al overproduction if combined with the metallicity enhancement. In fact, if ^{26}Al production by massive stars would indeed follow the $(Z/Z_{\odot})^2$ dependence predicted by non-rotating stellar models, a break-down of the tight correlation between 1.809 MeV and galactic free-free emission would be expected due to the inverse metallicity dependencies of both emission processes – the 1.809 MeV intensity should be enhanced in the metal-rich inner regions of the Galaxy due to enhanced ^{26}Al production, while the free-free emission should be reduced due to lower electron temperatures (see Knödseder 1999).

The existing data show no indication for such an anti-correlation. However, it is likely that rotation reduces the metallicity dependence of Wolf-Rayet star yields. The fact that at low metallicity, there is less ^{25}Mg , might be somewhat compensated by the fact that when the metallicity decreases, the mixing is more efficient, bringing more ^{25}Mg from the radiative envelope into the core and more ^{26}Al from the convective core into the radiative envelope. The mixing efficiency increases when the metallicity decreases because, when Z decreases, the stars are more compact, the internal gradients of the angular velocity are steeper and the stars loose less angular momentum by mass loss through stellar winds (see Maeder & Meynet 2001). Secondly, when rotation is accounted for, the mass loss rate plays a less important role in the WR formation process (see Fig. 6). Thirdly, at low metallicity, stars loose less angular momentum. As a consequence they can more easily reach the break-up limit at a given stage during their evolution. Very high mass loss rates ensue even if the metallicity is low. Finally, there are some indirect indications, that the proportion of fast rotators increases when the metallicity decreases (Maeder et al. 1999).

Since rotation seems to erode the metallicity dependence of Wolf-Rayet star yields, it provides an appealing mechanism to explain the absence of a 1.809 MeV – free-free emission anti-correlation. Remains to be seen if rotation can also be a solution to the ^{26}Al yield puzzle – both for the Cygnus region and the Galaxy as a whole.

Acknowledgements. This research has made use of the SIMBAD database, operated at CDS, Strasbourg, France and the WEBDA database, compiled by Jean-Claude Mermilliod, Institute of Astronomy of the University of Lausanne, Switzerland.

Appendix A: OB associations

A.1. Cep OB1

Our data are based on the work of Garmany & Stencel (1992) complemented by early type stars within the field of the association that we extracted from the SIMBAD database. The large angular extent of $15^\circ \times 4^\circ$ together with a distance of 3.6 kpc implies linear dimensions of 950×250 pc, considerably larger than the typical size of OB associations (Garmany 1994). Already Moffat (1971) noted for this reason that Cep OB1 may be the combination of several OB associations. Indeed, the HRD suggests the existence of two subgroups of different age that we term Cep OB1a (2 – 5 Myr) and Cep OB1b (9 – 18 Myr). There are 4 WR stars in the field of Cep OB1 which are possibly associated to the young subgroup. However, the subgroups do not separate spatially into two distinct groups but are rather immersed into each other. Thus the large size of Cep OB1 still remains unexplained, and it is possible that Cep OB1 splits either into even more subgroups or that the stars are physically unrelated.

A.2. Cep OB2

Cep OB2 has been recently revisited by de Zeeuw et al. (1999) by means of *Hipparcos* data, and we based our analysis on their list of probable members. We complemented the *Hipparcos* data by spectroscopic information from the SIMBAD database, and carefully excluded possible members of the cluster Trumpler 37 from the dataset. The resulting HRD shows a relatively nice main sequence, and our distance modulus of 9.1 ± 0.3 mag agrees well with the *Hipparcos* value of 8.9 mag (de Zeeuw et al. 1999). However, in contrast to de Zeeuw et al. (1999), we do not confirm a physical relation between the association and the open clusters NGC 7160 and Trumpler 37 since both lie at significantly larger distances.

A.3. Cyg OB1

The Cyg OB1 association spatially overlaps with the young open clusters Berkeley 86, Berkeley 87, IC 4996, and NGC 6913, and we will argue below that all four clusters are likely physically related to the association. We based our stellar census on the compilations of Garmany & Stencel (1992) and Zakirov (1999) which include also member stars from the open clusters. Stars that coincide spatially with one of these clusters have therefore been excluded and put in the respective cluster database. Conversely, stars from the cluster databases that are located outside the classical cluster boundaries were included in the Cyg OB1 list. We added spectroscopic information from the SIMBAD database and added also the Wolf-Rayet stars that are likely associated to Cyg OB1 (van der Hucht 2001). The resulting HRD shows a clear

though slightly broad main sequence, and the relatively flat IMF slope of $\Gamma = -1.0$ suggests that our database is probable not complete for low mass stars.

A.4. Cyg OB2

Cyg OB2 is one of the most massive stellar associations known in our Galaxy and houses about ~ 120 O type stars (Knödlseider 2000). We based our analysis on the spectrophotometric survey of Massey & Thompson (1991) although we recognise that their observations cover only the central part of the association area. We therefore adopt the results from Knödlseider (2000) for the total mass normalisation, yet rely on the more precise spectroscopic information from Massey & Thompson (1991) for the determination of the remaining association parameters. We added the three Wolf-Rayet stars WR144, 145, and 146 that coincide spatially with Cyg OB2 to the database, although their physical relation to the association is not established (van der Hucht 2001). The resulting HRD shows a nice and clearly defined main sequence (cf. Fig. 1). Our association parameters agree well with those found in other studies (e.g. Massey & Thompson 1991, Torres-Dodgen et al. 1991).

A.5. Cyg OB3

For Cyg OB3 our analysis is based on the compilation of Garmany & Stencel (1992) complemented by spectroscopic data from the SIMBAD database. On basis of spatial location possible members of the open clusters NGC 6871 and Biurakan 2 were excluded, and inversely, possible non-members of both clusters were included in the Cyg OB3 database. We also added the Wolf-Rayet stars WR134 and 135 (van der Hucht 2001). The resulting HRD is rather sparse yet shows a moderately well defined main sequence which, however, lacks low mass association stars. As consequence we obtain formally an extremely flat IMF slope of $\Gamma = -0.3 \pm 0.4$ which is probably heavily biased by the incompleteness of our database for faint stars (this should however not affect our nucleosynthesis predictions since only massive stars will contribute significantly to the yields).

A.6. Cyg OB7

The data for this extremely sparse association are again based on the list of Garmany & Stencel (1992) complemented by spectroscopic information from the SIMBAD database. Based on an analysis of *Hipparcos* data de Zeeuw et al. (1999) argues that Cyg OB7 is likely a chance projection of massive stars since no common motion has been detected for the members (the authors draw the same conclusion for Cyg OB4). Our HRD shows a very sparsely populated yet reasonably narrow main sequence, therefore we kept the association in our list of massive star populations.

A.7. *Cyg OB8*

The data for this association were compiled from Humphreys (1978) and the SIMBAD database. The HRD is extremely sparse and no clear main sequence can be identified, making the physical reality of this association extremely doubtful. We reflect this uncertainty by attributing a large age uncertainty (1 – 14 Myr) to Cyg OB8.

A.8. *Cyg OB9*

Our database was compiled from the list of Garmany & Stencel (1992) complemented by spectroscopic information from SIMBAD. Possible members of NGC 6910 have been excluded from the list based on spatial location. The HRD of this association is rather sparse, yet a broad main sequence is perceptible which indicates an age spread of 2 – 5 Myr.

A.9. *Lac OB1*

The nearby association Lac OB1 has been recently studied by de Zeeuw et al. (1999) using *Hipparcos* data, and we based our analysis on their list of likely members, complemented by SIMBAD data. Lac OB1 shows a reasonably well defined main sequence with a turn-off age around 12 – 15 Myr. There is one star deviating from the main sequence at the bright end (10 Lac) and it is questionable if this star is physically related to the association (the *Hipparcos* parallax places this star at the near side of the association). The most intriguing discrepancy with respect to the study of de Zeeuw et al. (1999) is the distance estimate towards the association. The *Hipparcos* parallax measurement of 368 ± 17 pc translates into a distance modulus of 7.8 ± 0.1 mag while we obtained a significantly larger value of 9.0 ± 0.5 mag. De Zeeuw et al. (1999) pointed already out that their distance estimate is significantly smaller than most spectrophotometric estimates, but attributed this discrepancy to the significant modification of the list of members in their work. We cannot confirm this hypothesis since we used the same member list as de Zeeuw et al. (1999) and still find a significantly larger distance estimate for Lac OB1.

A possible explanation of this discrepancy may come from the fact that most MK classified stars in Lac OB1 are of spectral type B2-3. In this spectral domain the absolute visual magnitude M_V varies extremely rapidly with spectral type (see e.g. Fig. 1a of de Geus 1990) and consequently the absolute luminosity of these stars is only poorly defined. Comparison of our Lac OB1 data to the *Hipparcos* parallaxes suggests that absolute magnitude estimates for B2-3 V stars are about 1.4 mag too bright. It is not clear to us if this overestimation is due to a spectral misclassification of the stars (which seems unlikely due to the high number of stars involved), due to the insufficiency of the stellar calibrations (we used the calibrations of Humphreys & McElroy 1984 and Schmidt-Kaler 1982),

or due to a subtle effect of stellar rotation (e.g. Lamers et al. 1997; however we did not find any dependence of luminosity overestimation on rotational velocity). We note, however, that it appears as a general feature in the analysis of our stellar populations that stars in this spectral domain tend to be too bright (see for example Fig. 1 which shows the same trend for stars with $\log T_{\text{eff}} \sim 4.3$ in Cyg OB2). It is however not within the scope of the present paper to revise the absolute magnitude calibration for early B-type stars, but it is obvious that there is a pressing need for a detailed look at this problem (e.g. Massey et al. 1995).

A.10. *Vul OB1*

For Vul OB1 our database is based on the compilation of Garmany & Stencel (1992), complemented by spectroscopic information from SIMBAD. From their spatial location possible members of NGC 6823 have been excluded from the list. The HRD of this association is rather sparse, and no clear main sequence is perceptible. The physical reality of Vul OB1 is therefore highly questionable.

Appendix B: Open clusters

B.1. *Berkeley 86*

Berkeley 86 has been proposed by Blaha & Humphreys (1989) as one of the three nuclei of Cyg OB1, the others being NGC 6913 and IC 4996. The WEBDA data on Berkeley 86 are contaminated by stars of the Cyg OB1 association and the cluster IC 4996, hence a careful separation of these stars has been conducted on basis of stellar positions. The resulting cluster parameters are compatible with the values found in the literature (e.g. Deeg & Ninkov 1996). The distance modulus, reddening, and age of Berkeley 86 is in agreement with the parameters of Cyg OB1, supporting its physical connection to the association. There is one Wolf-Rayet star in the field of Berkeley 86 (WR139), an eclipsing binary system of type WN5 - O6III-V (van der Hucht 2001). Our age estimate of 3 – 5 Myr is compatible with the physical association of the system to the cluster.

B.2. *Berkeley 87*

For Berkeley 87, the data in the WEBDA database are essentially based on the UBV photometric survey of Turner & Forbes (1982) and the spectroscopic observations of Massey et al. (2001). From the former data the authors determined a distance modulus of 9.88 mag for the cluster, while the new spectroscopic data of Massey et al. (2001) suggest a high value of 11.0 mag. We also find a high distance modulus of 11.4 mag for the combination of all available data, which places Berkeley 87 at the same distance as the Cyg OB1 association. The spatial overlap with Cyg OB1 makes it highly likely that Berkeley 87 is indeed physically connected to this associ-

ation. Among all clusters that we examined, Berkeley 87 shows the highest reddening ($E(B-V) = 1.63$), reflecting the heavy obscuration by a large molecular cloud complex in this area. Berkeley 87 houses one of the rare type WO2 Wolf-Rayet stars (WR142) near its centre (van der Hucht 2001), and our age estimate of 3–6 Myr seems compatible with the existence of such an object in the cluster.

B.3. Berkeley 94 and 96

Only photometric data are available for the two clusters from which we infer a distance modulus of 13.6 mag for both.

B.4. Biurakan 2

For Biurakan 2, we supplemented the WEBDA data with spectroscopic information from the SIMBAD database. We removed stars number 126 and 131 from the list since their location in the $E(B-V)$ versus DM diagram clearly identifies them as foreground objects. Our resulting distance modulus of 11.8 mag is in excess to other works (e.g. Dupuy & Zukauskas 1976), which is mainly explained by the removal of stars number 126 and 131. We note that Biurakan 2 lies at the edge of the Cyg OB3 and its distance modulus and reddening are compatible with the parameters of this association. Yet, our age estimate of 24–30 Myr makes their physical relation questionable.

B.5. IC 4996

IC 4996 is situated in the field of Cyg OB1 and has been suggested as nuclei of the association (Garmany & Stencel 1992, and references therein). Our cluster parameters corroborate this hypothesis.

B.6. IC 5146

The cluster IC 5146 is related to a spherical emission-reflection nebula which is excited by the most massive star in the field, the B1V star BD+46°3474 (e.g. Wilking et al. 1984). The WEBDA database for IC 5146 is heavily contaminated by fore- and background stars, and severe boundaries on $E(B-V)$ were necessary to extract the cluster stars. The resulting HRD is very sparsely populated, with BD+46°3474 being the only massive object. Indeed, for this star we derive a distance modulus of 9.2 mag while the average cluster distance amounts to 10.3 mag. Excluding BD+46°3474 results in an even larger DM of 10.8 ± 0.3 mag, suggesting that BD+46°3474 may indeed lie in front of the cluster. In this case, the earliest spectral type in IC 5146 would be as late as B8V, making it too old for our purpose. We therefore excluded the cluster from the analysis.

B.7. NGC 6823

NGC 6823 is an extremely rich cluster for which abundant photometric and spectroscopic information is available. The colour-colour diagram of the database shows a very broad main sequence between $0.5 < E(B-V) < 1.2$, illustrating the variable extinction in this area. Indeed, NGC 6823 lies in the middle of the moderately bright H II region NGC 6820, and variable extinction is common in such a configuration. NGC 6823 is proposed as the nucleus of the Vul OB1 association, and indeed our cluster parameters agree well with that of the association.

B.8. NGC 6871

NGC 6871 has been suggested as nucleus of the Cyg OB3 association (e.g. Garmany & Stencel, 1992) and the WEBDA database for this cluster contains a substantial number of association members but also field stars. From their spatial and evolutionary parameters, roughly 20 stars were excluded from the WEBDA list and included in the Cyg OB3 database, yet we admit that this membership assignment is a rather arbitrary process. Nevertheless, Cyg OB3 and NGC 6871 have very similar distances and ages, and we could probably have treated both as a single object. The WEBDA data have been complemented with spectral types from Massey et al. (1995) and from the SIMBAD database. Near the centre of NGC 6871 we find the type WN5 Wolf-Rayet star WR133 (van der Hucht 2001). Our age estimate of 5–6 Myr is compatible with the presence of such an object in NGC 6871.

B.9. NGC 6883

The WEBDA database contains only UBV magnitudes for 9 stars in this cluster resulting in a sparsely populated main sequence. The earliest spectral type in the cluster is B1III. NGC 6883 lies at the edge of Cyg OB3 and the cluster reddening is similar to that of the association. Yet the cluster is marginally closer than Cyg OB3, and in particular the age estimate is not compatible with a contemporaneous formation of both stellar groups. We therefore consider a physical relation as doubtful.

B.10. NGC 6910

NGC 6910 lies at the edge of the Cyg OB9 association, yet their physical relation is questioned by their significantly different distance moduli (see also Garmany & Stencel 1992). We removed a small fraction of the stars in the WEBDA database due to their particular low $E(B-V)$ values, and updated spectral types from the SIMBAD database.

B.11. NGC 6913

This young open cluster, also known as M29, is situated in the field of Cyg OB1 and is considered as one

of the nuclei of this association. Wang & Hu (2000) recently obtained spectroscopic observations of 100 probable cluster members from which they derived a distance modulus of 10.17 mag, much closer than the estimate of Massey et al. (1995) of 11.71 mag based on spectroscopic data. We examined both the Massey et al. (1995) and Wang & Hu (2000) datasets and found that the latter is probably biased by pre-main sequence and foreground stars. As noted by Wang & Hu (2000), many stars in their sample show an abnormal reddening slope, hence we excluded all objects with q_r outside the interval 0.5 – 1.5 from the dataset. Already this simple selection increases the distance modulus of the Wang & Hu (2000) dataset to 11.1 mag. Figure 6 in Wang & Hu (2000) shows that only stars with $0.9 < E(B - V) < 1.2$ show a spatial concentration to the cluster centre. Using the more relaxed condition $0.6 < E(B - V) < 1.5$ we obtain a distance modulus of 11.3 ± 1.0 mag, while the more severe restriction $0.9 < E(B - V) < 1.2$ results in 11.7 ± 0.6 mag. We therefore adopt a distance of 11.3 ± 1.0 mag for NGC 6913 which places the cluster at the same distance as Cyg OB1, strengthening the hypothesis of being a nuclei of this association.

B.12. NGC 7067

For this poor cluster spectroscopic information is only available for three stars (numbers 2, 4, and 5) in the WEBDA database. However, our analysis suggests that these three stars are all foreground objects that are superimposed on the cluster area. Excluding these stars results in a rather large distance modulus of 14.2 mag.

B.13. NGC 7128

NGC 7128 has been recently studied by Balog et al. (2001) who determined a distance modulus of 13.0 ± 0.2 mag and an age above 10 Myr. The WEBDA database for this cluster contains spectroscopic information for four stars which again are considerable closer than the remaining cluster stars. Thus, we excluded these four objects from the analysis which resulted in a distance modulus and reddening that is agreement with the analysis of Balog et al. (2001).

B.14. NGC 7160

The WEBDA database contains photometric and spectroscopic information for this cluster. We exclude stars number 407 and 487 from the list since they are too far from the cluster centre. NGC 7160 has been discussed as possible nuclei of Cep OB2 (Garmany & Stencel 1992), but our distance modulus estimate places the cluster behind this association.

B.15. NGC 7235

The WEBDA database for this cluster is heavily contaminated by non-members which we tried to exclude by applying reddening selections. The very steep IMF slope of $\Gamma = -2.6$ indicates that we probably did not fully succeed in eliminating faint non-member stars from the database. NGC 7235 lies at the edge of the Cep OB1 association and indeed our distance modulus estimates for both objects are fairly compatible. Our age estimate of 4 – 5 Myr suggests a possible physical relation to the young subgroup of the association (Cep OB1a).

B.16. NGC 7261

NGC 7261 is another cluster at the edge of the Cep OB1 association, and our distance estimate again suggests that both objects could be physically related. Our age estimate of 12 – 20 Myr suggests that NGC 7261 is related to the old subgroup of the association (Cep OB1b).

B.17. NGC 7380

The young open cluster NGC 7380 is associated with a bright H II region, and as often in such a configuration, there is a large scatter in extinction of the cluster stars, ranging from $0.5 < E(B - V) < 0.9$. We excluded a few stars from the WEBDA database since they were too far from the cluster centre and/or their reddenings did not correspond to the reddenings found in their vicinity. A reddening selection was applied to reject further non-members. NGC 7380 also lies in the field of Cep OB1, and all cluster parameters (reddening, distance, age) are compatible with a physical relation to the young subgroup (Cep OB1a).

B.18. Roslund 4

Roslund 4 is a small open cluster for which the WEBDA database contains 12 objects (stars number 13 and 14 have been removed since they are local photoelectrical standards and are not part of the cluster). Our distance estimate is identical to that of Racine (1969), which is no surprise since we used the same data. No spectroscopic information is available for the stars in Roslund 4, making an age estimate rather difficult. From the luminosity and temperature of the most massive stars in the cluster ($\sim 10 M_{\odot}$) we infer a highly uncertain age in the range 5 – 15 Myr.

B.19. Roslund 5

The WEBDA data have been complemented by spectral types from the SIMBAD database and membership data from Baumgardt (1998). Our distance estimate of 8.6 ± 0.3 agrees nicely with the *Hipparcos* value of 8.6 ± 0.4 (Baumgardt 1998). The earliest star in the cluster is of spectral type B3V and based on the location of this star

in the HRD we estimate an age between 20 – 30 Myr for this cluster.

B.20. Ruprecht 175

The WEBDA database for Ruprecht 175 is based on the work of Turner (1998) and contains, as the author states, a large fraction of probable non-member stars. Based on his Table 5, we selected probable cluster members from the database, resulting in a distance modulus of 11.3 mag for Ruprecht 175. In contrast, Turner (1998) obtained a distance modulus of only 10.4 mag. Our distance estimate is based on the 3 stars with spectroscopic information in the database which all show a distance modulus around 11.3 mag. Turner (1998) added also photometric data which systematically show smaller distance moduli, pushing the mean cluster distance to a lower value. Due to the high uncertainties involved in photometric distance estimates, we prefer the spectroscopic distance, although it is only based on a small sample of stars. The earliest star in Ruprecht 175 is of spectral type B3V and based on the location of this star in the HRD we estimate an age between 20 – 30 Myr for this cluster.

B.21. Trumpler 37

Trumpler 37 is embedded in the centre of the bright H II region IC 1396, and is suggested to form the nucleus of the Cep OB2 association. The cluster has been studied by numerous authors, and consequently, there is a rich database of stellar data available. The WEBDA database contains a substantial fraction of non-members which we exclude by means of reddening selections. Our distance modulus of 10.2 ± 0.4 mag is consistent with other works (e.g. Garrison & Kormendy 1976) and agrees in particular with the *Hipparcos* estimate of 9.9 ± 0.8 mag (Robichon et al. 1999). This distance is significantly larger than our estimate of 9.1 ± 0.3 mag for Cep OB2, rejecting claims that Trumpler 37 is physically related to this association (e.g. de Zeeuw et al. 1999). Only an abnormally high ratio of absolute-to-selective absorption of $R_V \simeq 5$ would bring Trumpler 37 to a distance that is compatible with that of Cep OB2, yet a variable extinction analysis of the cluster stars results in $R_V = 3.0 \pm 0.3$, compatible with our assumption of $R_V = 3.1$ (see also Morbidelli et al. 1997). We therefore conclude that it is unlikely that Trumpler 37 is indeed physically related to Cep OB2. Our age estimate of 3–6 Myr encompasses determinations by other authors (e.g. Clayton & Fitzpatrick 1987; Marschall et al. 1990).

References

- Afflerbach, A., Churchwell, E., & Werner, M. W. 1997, *ApJ*, 478, 190
- Arnould, M., Paulus, G., & Meynet, G. 1997, *A&A*, 321, 452
- Balog, Z., Delgado, A. J., Moitinho, A., et al. 2001, *MNRAS*, 323, 872
- Baumgardt, H. 1998, *A&A*, 340, 402
- Bennett, C. L., Smoot, G. F., Hinshaw, G., et al. 1992, *ApJ*, 396, L7
- Blaha, C., & Humphreys, R. M. 1989, *AJ*, 98, 1598
- Bochkarev, N.G., & Sitnik, T.G. 1985, *ApSS*, 108, 237
- Braun, H., & Langer, N. 1995, *A&A*, 297, 483
- Cash, W., Garmire, G., & Riegler, G. 1980, *ApJ*, 238, L71
- Cerviño, M., Knödseder, J., Schaerer, D., von Ballmoos, P., & Meynet, G. 2000, *A&A*, 363, 970
- Clayton, G. C., & Fitzpatrick, E. L. 1987, *AJ*, 92, 157
- Comerón, F., Torra, J., Jordi, C., & Gómez, A. E. 1993, *A&AS*, 101, 37
- Comerón, F., & Torra, J. 1994, *ApJ*, 423, 652
- Comerón, F., Torra, J., & Gómez, A. E. 1998, *A&A*, 330, 975
- Conti, P. S., & Blum, R. D. 2002, *ApJ*, 564, 827
- Daflon, S., Cunha, K., Becker, S. R., & Smith, V. V. 2001, *ApJ*, 552, 309
- Deeg, H. J., & Ninkov, Z. 1996, *A&AS*, 119, 221
- de Jager, C., Nieuwenhuijzen, H., & van der Hucht, K. A. 1988, *A&AS* 72, 259
- Del Rio, E., von Ballmoos, P., Bennett, K., et al. 1996, *A&A*, 315, 237
- De Geus, E. J. 1990, In *Properties of hot luminous stars; Proceedings of the First Boulder-Munich Workshop*, Boulder, CO, Aug. 6-11, 1988 (A90-36851 15-90). San Francisco, CA, Astronomical Society of the Pacific, 1990, p. 3-15.
- De Zeeuw, P. T., Hoogerwerf, R., de Bruijne, J. H. J., Brown, A. G. A., & Blaauw, A. 1999, *AJ*, 117, 354
- Diehl, R., Dupraz, C., Bennett, K., et al. 1995, *A&A*, 298, 445
- Dupuy, D. L., & Zukauskas, W. 1976, *Journal of the Royal Astronomical Society of Canada*, 70, 169
- Dutra, C. M., & Bica, E. 2001, *A&A*, 376, 434
- Ferguson, A. M. N., Wyse, R. F. G., Gallagher, J. S., & Hunter, D. A. 1996, *AJ*, 111, 2265
- Figer, D. F., Kim, S. S., Morris, M., et al. 1999, *ApJ*, 525, 750
- FitzGerald, M. P. 1970, *A&A*, 4, 234
- Garmany, C. D. 1994, *PASP*, 106, 25
- Garmany, C. D., & Stencel, R. E. 1992, *A&AS*, 94, 211
- Garmany, C. D., Conti, P. S., & Chiosi, C. 1982, 263, 777
- Garrison, R. F., & Kormendy, J. 1976, *PASP*, 88, 865
- Herrero, A., Corral, L. J., Villamariz, M. R., & Martin, E. L. 1999, *A&A*, 348, 542
- Hoogerwerf, R., Bruijne, J. H. J., & de Zeeuw, P. T. 2001, *A&A*, 365, 49
- Huchtmeier, W. K., & Wendker, H. J. 1977, *A&A*, 58, 197
- Humphreys, R. M., & McElroy, D. B. 1984, *ApJ*, 284, 565
- Humphreys, R. M. 1978, *ApJS*, 38, 309
- Hunter, D. A., & Massey, P. 1990, *AJ*, 99, 846
- Inoue, A. K., Hirashita, H., & Kamaya, H. 2001, 555, 613
- Knödseder, J., & Vedrenne, G. 2001, in: *Exploring the Gamma-Ray Universe*, eds. A. Gimenez, V. Reglero, & C. Winkler, p. 23
- Knödseder, J. 2000, *A&A*, 360, 539
- Knödseder, J., Bennett, K., Bloemen, H., et al. 1999a, *A&A*, 344, 68
- Knödseder, J., Dixon, D., Bennett, K., et al. 1999b, *A&A*, 345, 813
- Knödseder, J. 1999, *ApJ*, 510, 915
- Lamers, H. J. G. L. M., Harzevoort, J. M. A. G., Schrijver, H., et al. 1997, *A&A*, 325, L25
- Lamers, H., & Cassinelli, J. P. 1996, *Mass Loss from Stars*. In: Leitherer C., Fritze-von-Alvensleben U., Huchra J. (eds.) *From Stars to Galaxies: The Impact of Stellar Physics on Galaxy Evolution*. ASP Conf. Series 98, p. 162

- Langer, N. 1998, *A&A* 329, 551
- Langer, N., Braun, H., & Wellenstein, S. 1998, in: Proceedings of the 9th Workshop on Nuclear Astrophysics, eds. W. Hillebrandt & E. Müller, p. 18
- Le Duigou, J. M., & Knödlseeder, J. 2002, *A&A*, submitted
- Maeder, A., & Meynet, G. 2001, *A&A*, 373, 555
- Maeder, A., & Meynet, G. 2000, *A&A*, 361, 159
- Maeder, A., Grebel, E., & Mermilliod, J. C. 1999, *A&A* 346, 459
- Maeder, A., & Meynet, G. 1994, *A&A*, 287, 803
- Maeder, A. 1992, *A&A*, 264, 105
- Marschall, L. A., Comins, N.F., & Karshner, G.B. 1990, *AJ*, 99, 1536
- Martins, F., Schaerer, D., & Hillier, D. J. 2002, *A&A*, 382, 999
- Massey, P., DeGioia-Eastwood, K., & Waterhouse, E. 2001, *AJ*, 121, 1050
- Massey, P., Johnson, K. E., & DeGioia-Eastwood, K., et al. 1995, *ApJ*, 454, 151
- Massey, P., & Thompson, A. B. 1991, *AJ*, 101, 1408
- Mathis, J.S. 1990, *ARAA*, 28, 37
- Mermilliod, J.-C. 1998, *Bull. Inform. CDS* 35, 77-91
http://obswww.unige.ch/webda/webda.html
- Meynet G., & Maeder A. 2000, *A&A*, 361, 101
- Meynet, G., Arnould, M., Prantzos, N., & Paulus, G. 1997, *A&A* 320, 460
- Meynet, G., Maeder, A., Schaller, G., Schaerer, D., & Charbonnel, C. 1994, *A&AS* 103, 97
- Mezger, P. G., Smith, L. F., & Churchwell, E. 1974, *A&A*, 32, 269
- Moffat, A. F. J., Drissen, L., & Shara, M. M. 1994, *ApJ*, 436, 183
- Moffat, A. F. J. 1971, *A&A*, 13, 30
- Morbidelli, L., Patriarchi, P., Perinotto, M., Barbaro, G., & di Bartolomeo, A. 1997, *A&A*, 327, 125
- Oey, M. S., & Kennicutt, R. C. Jr. 1998, *PASA*, 15, 141
- Oey, M. S., & Kennicutt, R. C. Jr. 1997, *MNRAS*, 291, 827
- Panagia, N. 1973, *AJ*, 78, 929
- Parthasarathy, M., Jain, S. K., & Bhatt, H. C. 1992, *A&A*, 266, 202
- Pigulski, A., & Kolaczowski, Z. 1998, *MNRAS*, 298, 753
- Plüschke, S. 2001, PhD thesis, MPE
- Prantzos, N., & Diehl, R. 1996, *Phys. Rep.*, 267, 1
- Racine, R. 1969, *AJ*, 74, 816
- Ringger, D. 2000, Diploma work, Lausanne University
- Robichon, N., Arenou, F., Mermilliod, J.-C., & Turon, C. 1999, *A&A*, 345, 471
- Schaerer, D. 1999, in: Stars, Gas and Dust in Galaxies: Exploring the Links, eds. D. Alloin, G. Galaz, K. Olsen, ASP Conf. Series, 221, 99
- Schaerer, D. 1999, in: Boulder Munich Workshop II: Properties of Hot Luminous Stars, ed. I. Howarth, ASP Conf. Series, 131, 310
- Schaerer, D., & de Koter, 1997, *A&A*, 322, 598
- Schmidt-Kaler, T. 1982, *Landolt-Börnstein*, VI, Vol. 2, 453
- Schmutz, W., Leitherer, C., & Gruenwald, R. 1992, *PASP*, 104, 1164
- Sodroski, T. J., Odegard, N., Arendt, R. G., et al. 1997, *ApJ*, 480, 173
- Torres-Dodgen, A. V., Tapia, M., & Carroll, M. 1991, *MNRAS*, 249, 1
- Turner, D. G. 1998, *AJ*, 118, 274
- Turner, D. G., & Forbes, D. 1982, *PASP*, 94, 789
- Uyaniker, B., Fürst, E., Reich, W., Aschenbach, B., & Wielebinski, R. 2001, *A&A*, 371, 675
- Vacca, W. D., Garmany, C. D., & Shull, J. M. 1996, *ApJ*, 460, 914
- van der Hucht, K. A. 2001, *New Astronomy Reviews*, 45, 135
- Wang, J.-J. & Hu, J.-Y. 2000, *A&A*, 356, 118
- Wendker, H. J., Higgs, L. A., & Landecker, T. L. 1991, *A&A*, 241, 551
- Wendker, H. J. 1970, *A&A*, 4, 378
- Wilking, B. A., Harvey, P. M., & Joy, M. 1984, *AJ*, 89, 496
- Woolsey, S., & Weaver, T. A. 1995, *ApJS*, 101, 181
- Woolsey, S., Langer, N., & Weaver, T. A. 1995, *ApJ*, 448, 315
- Zakirov, M. M. 1999, *Astron. Letters*, 25, 229